Ore Geology Reviews 84 (2017) 202–217

Contents lists available at ScienceDirect

Ore Geology Reviews

journal homepage: www.elsevier.com/locate/oregeo

Genesis of the Zhengguang gold deposit in the Duobaoshan ore field, Heilongjiang Province, NE China: Constraints from geology, geochronology and S-Pb isotopic compositions

Rongzhen Gao [a], Chunji Xue [a], Xinbiao Lü [b,c,*], Xiaobo Zhao [a], Yongsheng Yang [d], Chuncheng Li [b]

[a] State Key Laboratory of Geological Processes and Mineral Resource, School of Earth Sciences and Resources, China University of Geosciences, Beijing 100083, China
[b] Faculty of Earth Resource, China University of Geosciences, Wuhan 430074, China
[c] State Key Laboratory of Geological Processes and Mineral Resource, China University of Geosciences, Wuhan 430074, China
[d] Geological Survey Institute, China University of Geosciences, Wuhan 430074, China

ARTICLE INFO

Article history:
Received 4 July 2016
Received in revised form 22 December 2016
Accepted 23 December 2016
Available online 5 January 2017

Keywords:
S-Pb isotopes
Middle Ordovician
Zhengguang gold deposit
Duobaoshan
Central Asian Orogenic Belt

ABSTRACT

The Zhengguang gold deposit in the Duobaoshan ore field, hosted in volcanic rocks of the Middle Ordovician Duobaoshan Formation, is one of the largest gold deposits in the Northeastern Great Xing'an Range of the Central Asian Orogenic Belt (CAOB). The deposit comprises the No. I, II and III ore zones with a total resource exceeding 35 tonnes of Au, 100,000 tonnes of Zn and 100 tonnes of Ag. A genetic relationship between gold mineralization and concealed tonalite porphyry is inferred based on the characteristics of cryptoexplosive breccia and hydrothermal alteration indicative of porphyry-type and epithermal mineralization. Zircon LA-ICPMS U-Pb dating reveals that the tonalite porphyry was emplaced at 462.1 ± 1.8 Ma (Middle Ordovician). The $\delta^{34}S_{V\text{-}CDT}$ values of sulfide minerals range from −3.0‰ to −1.7‰ with an average of −2.33‰, indicating that sulfur was mainly derived from a magmatic source. The Pb isotopic compositions ($^{206}Pb/^{204}Pb$ ranging from 17.572 to 17.629, $^{207}Pb/^{204}Pb$ from 15.424 to 15.486, and $^{208}Pb/^{204}Pb$ from 37.206 to 37.418) suggest a major mantle component for Pb and, by inference, for other ore metals. Therefore, we suggest that the ore-forming elements in the Zhengguang gold deposit may be related to the mantle-sourced tonalite porphyry. On the basis of the geological characteristics and geochemical signatures documented in this study, we conclude that the Zhengguang gold deposit was formed in a porphyry to epithermal transitional environment associated with the concealed tonalite porphyry, as part of the Duobaoshan porphyry-epithermal ore system that is related to the subduction of the Paleo-Asian Ocean during the Ordovician.

1. Introduction

The Central Asian Orogenic Belt (CAOB) is regarded as the largest accretionary orogen in the world with remarkable crustal growth and formation of a great variety of mineral deposits during the Phanerozoic (Sengör et al., 1993; Pirajno, 2010; Xiao et al., 2013; Goldfarb et al., 2014; Mao et al., 2014; Seltmann et al., 2014; Zhang et al., 2016). While the magmatism and metallogeny of the CAOB during the late Paleozoic are well known, its ore-forming potential during the early Paleozoic remains relatively unclear (Goldfarb et al., 2014; Seltmann et al., 2014; Zhao et al., 2015). The Great Xing'an Range, situated in the eastern segment of the CAOB (Fig. 1), has experienced complex tectonic and extensive magmatism during the Paleozoic and Mesozoic (Ouyang et al., 2013; Bai et al., 2014; Wang et al., 2014; Wu et al., 2014). Most deposits in the Great Xing'an Range were formed during the Mesozoic tectono-magmatic activities related to the tectonic evolution of the Mongol-Okhotsk and Pacific oceans, e.g., the Wunugetushan Cu-Mo deposit (Wang et al., 2015), the Taipingchuan Cu-Mo deposit (Chen et al., 2010), and the Sandaowanzi Au deposit (Zhao et al., 2013). However, deposits with early Paleozoic ages have also been recognized in this region, such as the world-class Duobaoshan Cu-Mo-Au ore field (Zeng et al., 2014; Hao et al., 2015; Hu et al., 2016), which has a proven resource exceeding 3,350,000 tonnes of Cu, 150,000 tonnes of Mo and 100 tonnes of Au (Cui, 2006; Zhao et al., 2011a).

The Duobaoshan ore field hosts numerous deposits including the Duobaoshan and Tongshan porphyry Cu-Mo deposits, the Zhengguang Au deposit, the Sankuanggou skarn Fe-Cu deposit (Du et al., 1988; Liu et al., 2010a; Chen et al., 2012), the Jiguanshan

* Corresponding author at: Faculty of Earth Resources, China University of Geosciences, Lumo Road No.388, Hongshan District, Wuhan 430074, China.
E-mail addresses: Rongzhengao01@163.com (R. Gao), Lvxb_01@163.com (X. Lü).

http://dx.doi.org/10.1016/j.oregeorev.2016.12.031
0169-1368/

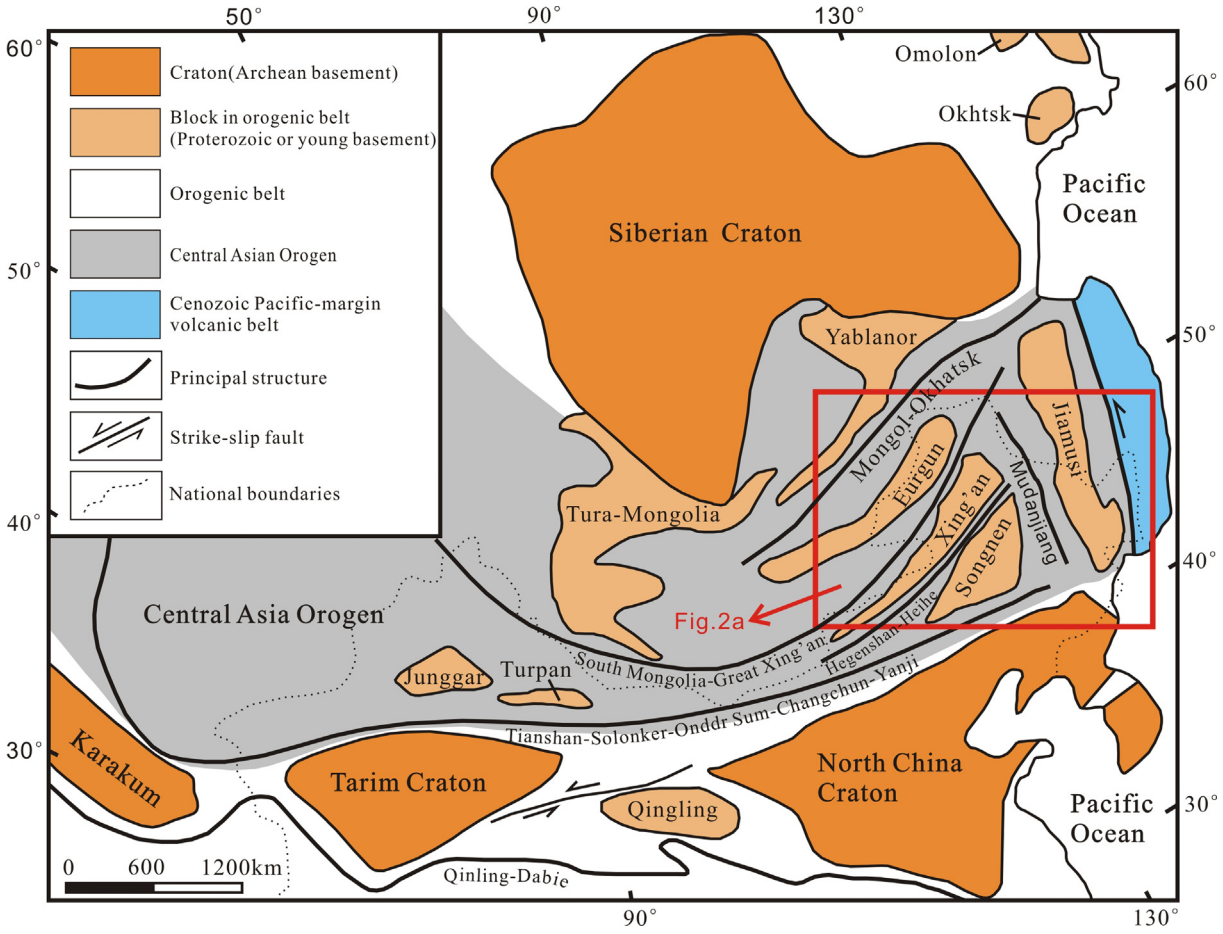

Fig. 1. Simplified tectonic map showing the main units of central and eastern Asia (modified after Zhou et al., 2011; Feng et al., 2015).

Mo deposit, as well as the Xiaoduobaoshan, Xiaogushan and Yuejin Cu deposits (Fig. 2b; Zhao and Zhang, 1997; Wu et al., 2009). These deposits change in mineralization style from skarn, porphyry to hydrothermal vein mineral systems from northwest to southeast (Zhao et al., 2011a). Porphyry mineralization of the early Paleozoic is partly reworked by tectono-magmatic processes of the late Paleozoic and Mesozoic (Zhao et al., 2011a). The Zhengguang gold deposit was discovered in 2006, and the initial exploration resulted

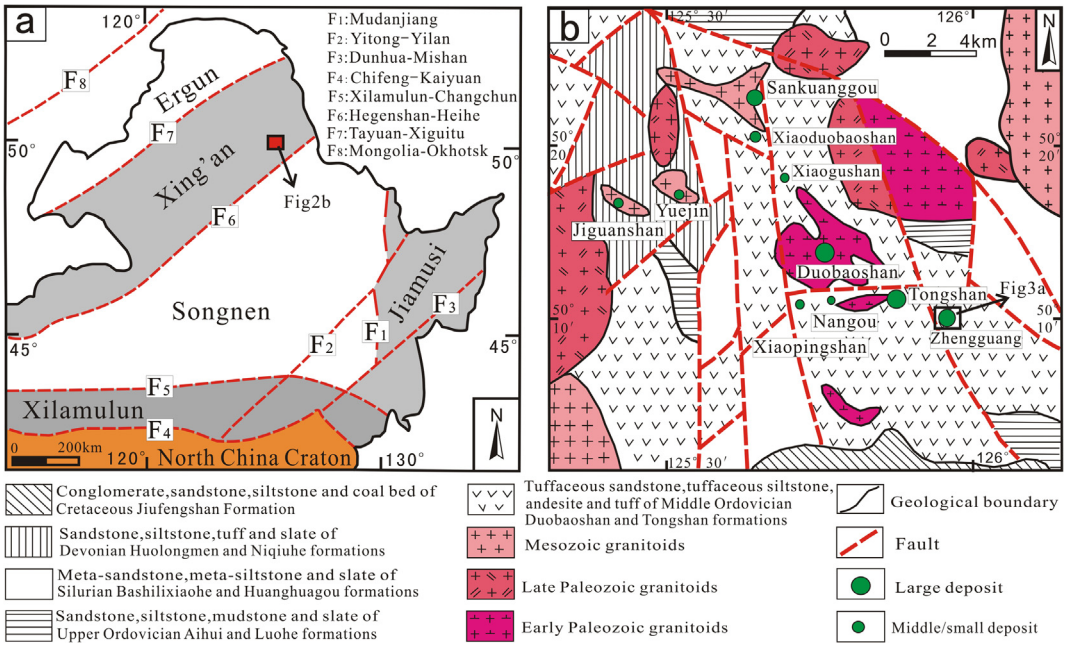

Fig. 2. Sketch tectonic map (a; after Ge et al., 2007) and simplified geological map (b; after Zeng et al., 2014; Hao et al., 2015) of the Duobaoshan ore field.

in an estimated resource of 12.6 tonnes of Au at an average grade of 3.49 g/t in the No. II ore zone (Deng et al., 2013). A significant breakthrough was achieved in the No. I ore zone by the Heilong Mining Corporation between 2010 and 2014, expanding the estimated resource to exceeding 35 tonnes of Au, 100,000 tonnes of Zn and 100 tonnes of Ag (Song et al., 2015).

A number of studies have been carried on the Zhengguang gold deposit, including general geology (Cui, 2006; Zhao et al., 2006, 2007; Lu and Liu, 2009; Fu and Yang, 2010; Gao et al., 2014a; Tong et al., 2015), fluid inclusions (Zhang et al., 2011; Deng et al., 2013; Gao et al., 2014b), C-H-O-S isotopes (Wu et al., 2006; Fu et al., 2014), geochronology (Fu et al., 2014; Shen et al., 2014; Li et al., 2016) and exploration criteria (Lu and Liu, 2009; Lu and Sun, 2015), all published in Chinese language literature. However, there are still many unanswered questions regarding the mineralization age and sources of ore-forming components. The mineralization age was considered to be Ordovician based on a zircon U-Pb age of 480.7 ± 3.2 Ma (Shen et al., 2014) from diorite dykes that are widely distributed in the No. II ore zone (Wu et al., 2006; Zheng, 2012; Fu and Yang, 2010), but the genetic relationship between the diorite and gold mineralization is still unclear. The Middle Ordovician Duobaoshan Formation in the area was regarded as the main source of the ore-forming components based on high concentrations of these elements in the strata (Wu et al., 2006; Fu and Yang, 2010), but there remains a lack of direct isotopic evidence. The genetic type of the Zhengguang gold deposit also remains controversial, having been classified as either a structure-controlled alteration rock type related to diorite (Wu et al., 2006; Zhao et al., 2007) or epithermal type (Zhang, 2004; Fu and Yang, 2010) including the low-sulfidation (Deng et al., 2013) and intermediate-sulfidation (Song et al., 2015) subtypes.

In this article, based on a detailed investigation of regional geological background and local geology, we demonstrate that the concealed tonalite porphyry in the Zhengguang Au deposit is genetically related to gold mineralization. The newly obtained zircon U-Pb dating results for the tonalite porphyry, together with new S-Pb isotope data of sulfides, are used to constrain the mineralization age and the sources of ore-forming materials. The significance of the study results on the Ordovician gold mineralization in the Duobaoshan porphyry-epithermal ore-forming system is discussed.

2. Geological background

The northeastern part of China, straddling the Siberian, North-China and Pacific plates, is regarded as a collage of several micro-continental blocks, namely the Ergun, Xing'an, Songnen and Jiamusi blocks (Fig. 2a; Ren et al., 1990). All of these blocks are separated by major faults, including the Tayuan-Xiguitu fault (F_7) between the Ergun and Xing'an blocks, the Hegenshan-Heihe fault (F_6) between the Xing'an and Songnen blocks, and the Mudanjiang fault (F_1) between the Songnen and Jiamusi blocks (Fig. 2a; Liu et al., 2010b; Wu et al., 2011; Xu et al., 2009). The Phanerozoic tectonic evolution involves closure of the Paleo-Asian Ocean, closure of the Mongol-Okhotsk Ocean and subduction of the Pacific Ocean (Wang and Mo, 1995; Wu et al., 2001; Jia et al., 2004; Hu et al., 2014a,b,c, 2016), with the structural framework being formed by the amalgamation of these micro-continental blocks from NW to SE (Fig. 2a; Wu et al., 2002, 2005, 2011; Hu et al., 2016). Although the ages and mechanisms of amalgamation remain controversial, it is generally agreed that the Xing'an block was accreted onto the Ergun block along the Tayuan-Xiguitu fault (F_7) during the early Paleozoic (She et al., 2012; Hu et al., 2014b, 2016), and the Songnen block was merged with the composite block along the Hegenshan-Heihe fault (F_6) during the late Paleozoic (Robinson et al., 1999; Chen et al., 2000; Wu et al., 2001, 2002, 2011; Gou et al., 2013). The final closure of the Paleo-Asian Ocean occurred from the late Permian to the early Triassic along the Xilamulun-Changchun fault (F_5), after which regional extension occurred (Xiao et al., 2003; Xu et al., 2009; Wu et al., 2011). This area then entered into an intraplate orogeny stage that was mainly controlled by the subduction of the Pacific Ocean during the Mesozoic (Wu et al., 2011; Mei et al., 2015). Besides, the Jiamusi block is regarded as an exotic block accreted onto the Asian continent along the Mudanjiang fault (F_1) during the Jurassic (Ge et al., 2007).

The Duobaoshan ore field is located in the Xing'an block on the northeastern part of the Hegenshan-Heihe fault (F_6) (Fig. 2a). It comprises 14 ore deposits and occurrences, including the Sankuanggou Fe-Cu deposit, the Duobaoshan and Tongshan Cu-Mo deposits and the Zhengguang Au deposit, and occurs within a structural zone of less than 40 km in extent (Fig. 2b; Deng et al., 2013). The Zhengguang Au deposit is the only gold deposit in the Duobaoshan ore field and it is situated 2 km from the Tongshan Cu-Mo deposit and 6 km from the Duobaoshan Cu-Mo deposit (Fig. 2b). The latest exploration has revealed a continuous NW-trending mineralization zone from the Duobaoshan Cu-Mo deposit to the Zhengguang Au deposit.

The lithologies in the Duobaoshan ore field are mainly Ordovician and Silurian, with minor Devonian and Cretaceous outcrops (Fig. 2b; Liu et al., 2012; Zeng et al., 2014; Hu et al., 2016). The Middle Ordovician Tongshan and Duobaoshan formations, which were considered to be the source of ore metals (Zhao et al., 2011b), are spatially related to the mineralization. The Tongshan Formation consists of terrigenous clastic rocks, whereas the Duobaoshan Formation comprises intermediate-felsic volcanic-volcanoclastic rocks (Du et al., 1988; Han et al., 2004; Zeng et al., 2014). The Upper Ordovician Aihui and Luohe formations are composed of sandstone, siltstone, mudstone and slate. The Silurian Bashilixiaohe and Huanghuagou formations comprise terrigenous clastic rocks and intermediate-mafic volcanic rocks. The Devonian Huolongmen and Niqiuhe formations consist of sandstone, silty sandstone, tuff and argilllic slate. The Cretaceous Jiufengshan Formation is composed of conglomerate, sandstone, siltstone and coal beds.

The area experienced multiple periods of intensive magmatism during the early Paleozoic, late Paleozoic and Mesozoic periods (Fig. 2b). The early Paleozoic granitoids, including the Duobaoshan and Tongshan granodiorite, were emplaced during the Ordovician with ages of 485–474 Ma (Ge et al., 2007; Cui et al., 2008; Xiang et al., 2012; Bai, 2013). The late Paleozoic granitoids are mainly alkali-feldspar granite and monzogranite emplaced during the Carboniferous-Permian with zircon U-Pb ages ranging from 311 to 291 Ma (Qu et al., 2011). The Mesozoic granitoids are mainly hornblende granodiorite and biotite granodiorite emplaced during the Jurassic with zircon U-Pb ages from 177 to 175 Ma (Ge et al., 2007; Chu et al., 2012). Mineralization in the Duobaoshan ore field is generally related to two major magmatic episodes: the Ordovician episode (e.g., the Duobaoshan Cu-Mo deposit) and the Jurassic episode (e.g., the Sankuanggou Fe-Cu deposit).

The mineral systems in the Duobaoshan ore field occur along the NW-trending Sankuanggou-Duobaoshan-Luohe structure zone, which consists of a series of transpressional strike-slip faults and minor folds (Zhao et al., 2011a). A large number of the NE- and nearly NS-trending faults are also present. These crosscutting structures form a complex fault network (Fig. 2b).

3. Geology of the Zhengguang gold deposit

3.1. Local geology

Lithologies in the Zhengguang gold deposit include the Tongshan and Duobaoshan formations. The former comprises a series

of terrigenous clastic rocks including andesitic tuff, tuffaceous sandstone and siltstone while the latter is composed of a series of littoral-shallow marine intermediate-felsic volcanic and volcaniclastic rocks including andesite, dacite, andesitic tuff, tuffaceous sandstone with interbedded siltstone, carbonaceous slate and a thin layer of volcanic breccia (Du et al., 1988; Han et al., 2004; Wu et al., 2005). The ore-bearing Duobaoshan Formation comprises three main units including, in ascending order, the first section comprising andesitic tuff and andesite, representing the main host rocks in the No. I ore zone, the second section composed of andesitic tuff, tuffaceous sandstone, andesite, carbonaceous slate and siltstone lamination, representing the main host rocks in the No. II ore zone, and the third section comprising andesitic tuff, andesite, rhyolite and dacite, representing the main host rocks in the No. II and III ore zones.

The area is characterized by a series of NW-, NE- and NNE-trending fractures and faults (Zhao et al., 2007). There are two major NW-trending faults occurring in the deposit (Fig. 3a): a high angle fault extending along the contact interface between the Duobaoshan and Tongshan formations and a second located within the Duobaoshan Formation, roughly paralleling with the first. The NW-trending faults are crosscut by the NE-trending faults.

Intrusions in the Zhengguang gold deposit consist of exposed diorite, diorite porphyry, dacite porphyry and a concealed tonalite porphyry. These intrusive bodies occur in the form of dykes or veins controlled by the NE-, NW- and nearly NS-trending faults in the area. The diorite locally hosts gold mineralization with a grade of more than 2 g/t, and was initially thought to be related to the gold mineralization by previous researchers (Wu et al., 2006; Zheng, 2012; Fu and Yang, 2010). However, the diorite dykes are crosscut by quartz-pyrite veins and the contact zone between the diorite and the Duobaoshan Formation is free of any alteration (Fig. 4a, 4b), indicating that the diorite is in fact not related to gold mineralization. Zircon U-Pb dating of the diorite yielded a crystallization age of 480.7 ± 3.2 Ma (Shen et al., 2014). The sporadically outcropping diorite porphyry yielded different zircon U-Pb ages of 291.7 ± 5.9 Ma (Song et al., 2015) and 478.3 ± 3.7 Ma (Li et al., 2016) by different authors, and the dacite porphyry in the Duobaoshan Formation has a zircon U-Pb age of 481 ± 3 Ma (Che et al., 2015).

The concealed tonalite porphyry was detected in the No. I ore zone by the latest exploration drill holes (e.g., ZK5808 and ZK4806), but its distribution, shape and size remain unclear. It is inferred that the tonalite porphyry occurs in the form of stocks or dykes, with its emplacement depth increasing from NE to SW from line 62 to line 42 in the No. I ore zone (Fig. 3a). The tonalite porphyry in the contact zone is pervasively altered and mineralized. In the drill core of ZK4806, the combined length of altered and mineralized intervals is >100 m over a total length of 193 m (Fig. 5). The tonalite porphyry, together with adjacent andesitic tuff or andesite in the Duobaoshan Formation, represents the most important host rocks. The tonalite porphyry is commonly crosscut by pyrite veinlets (Fig. 4c–f), quartz-polymetallic sulfide veins (Fig. 4e) and shows disseminated sulfide mineralization (Fig. 4c–f), whereas the neighbouring Duobaoshan Formation is characterized by intensive silicic, pyritic (Fig. 4c and d), and other hydrothermal alteration. K-feldspar alteration, mainly occurring as quartz-K-feldspar veins (Fig. 4e), is also locally developed in the tonalite porphyry bodies. The tonalite porphyry is grayish and has a porphyritic texture with 45–65% phenocrysts and 35–55% groundmass (Fig. 4g). The phenocryst consists of plagioclase, quartz, hornblende, biotite and K-feldspar while the microcrystalline groundmass is rich in plagioclase and quartz (Fig. 4g). The prismatic plagioclase has a characteristic polysynthetic twinning according to albite law and is commonly replaced by sericite and carbonate minerals (Fig. 4g and h). The round-shaped quartz is typically as large as 1 mm in length and the scaly biotite aggregation is usually as large as 1.5 mm (Fig. 4g). The platy hornblende has a characteristic 56° cleavage angle and show replacement by biotite (Fig. 4i). The tonalite porphyry has intensive pyritic (Fig. 4i and j), carbonate (Fig. 4j), and sericitic alteration (Fig. 4g and h).

3.2. Characteristics of orebodies

A total of 131 orebodies in the form of veins, lenses and pods have been delineated in the Zhengguang gold deposit, mainly

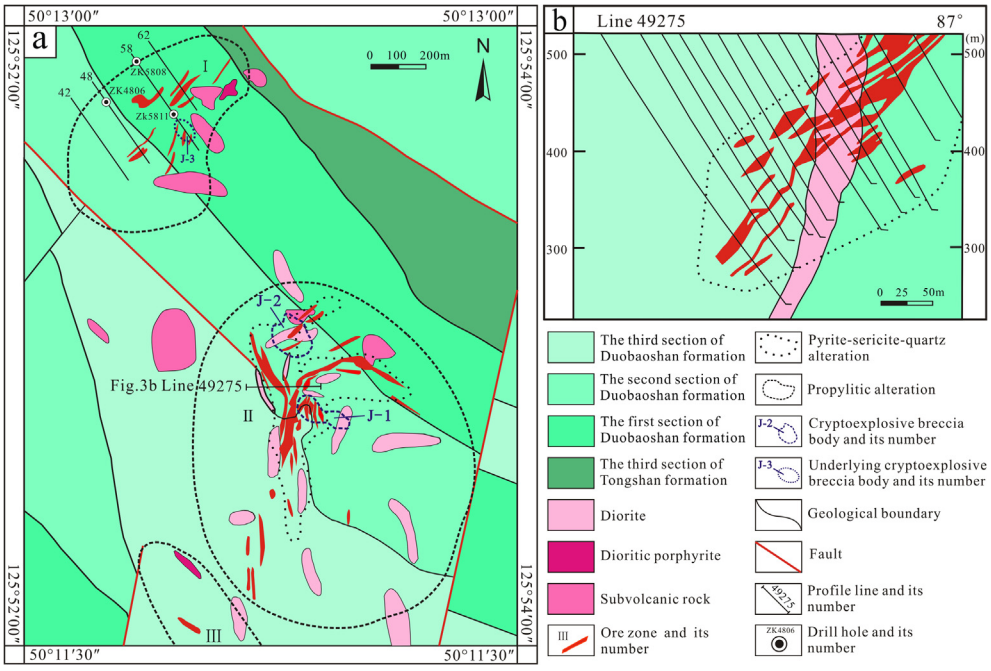

Fig. 3. Sketch geological map (a) and cross-section map for line 49275 of the No. II ore zone (b) in the Zhengguang Au deposit (modified after Zheng, 2012; Tong et al., 2015; Song et al., 2015).

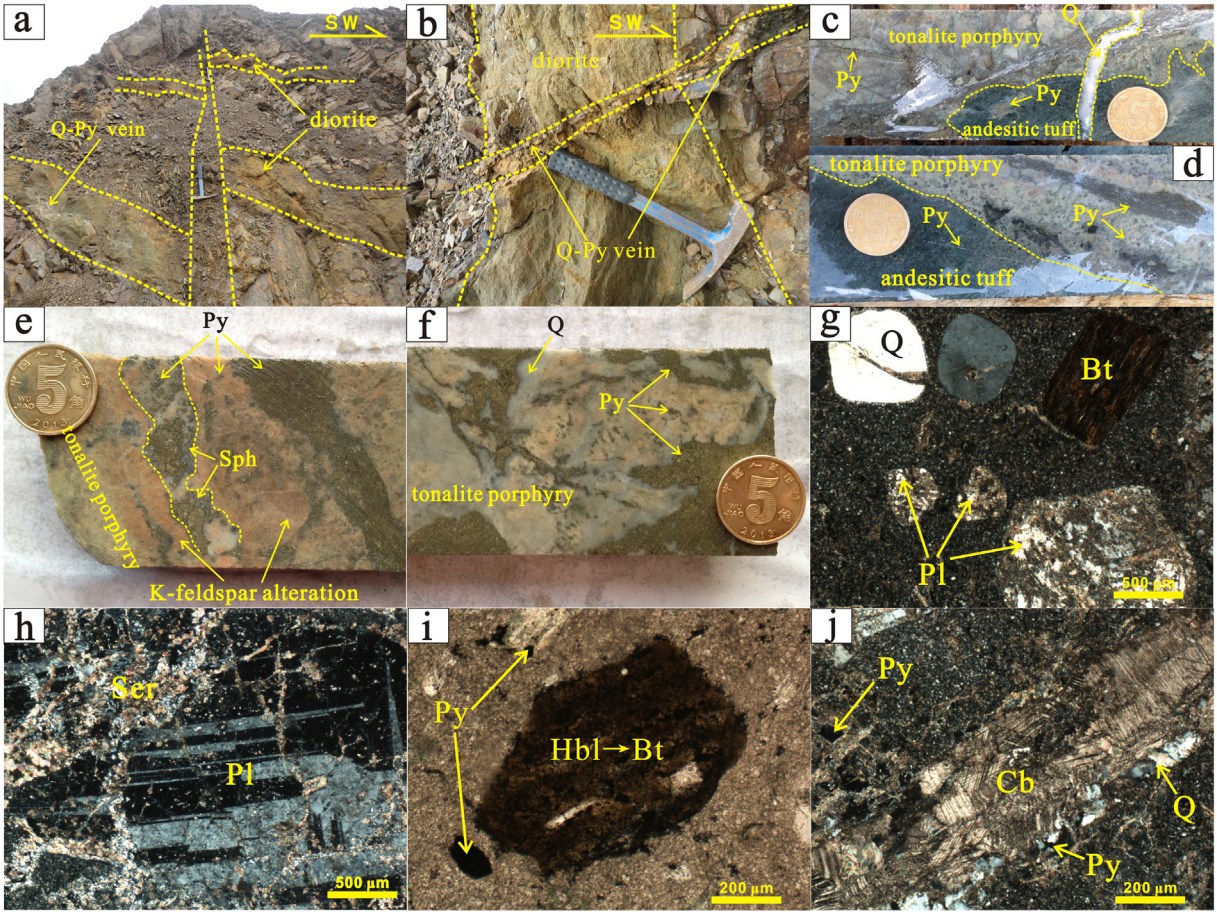

Fig. 4. Photographs showing the diorite dykes (a-b), mineralized tonalite porphyry (c-f), and photomicrographs showing the mineral assemblages and texture of the tonalite porphyry (g-j) in the Zhengguang Au deposit. (a) diorite dykes crosscut by NW-trending fracture and quartz-pyrite veins; (b) diorite dykes crosscut by quartz-pyrite veins; (c) brecciacious tonalite porphyry with fracture-filling pyrite veins and andesitic tuff with disseminated pyrite in the contact zone; (d) tonalite porphyry and andesitic tuff in the contact zone with veined and disseminated pyrite; (e) K-feldspar alteration in the tonalite porphyry and subsequent pyritic alteration, quartz-pyrite-sphalerite veins, and pyrite veins; (f) tonalite porphyry with intensive silicification and pyrite veins; (g) porphyritic texture with prismatic plagioclase, scaly aggregation of biotite and round-shaped quartz under cross-polarized light; (h) plagioclase phenocryst with polysynthetic twinning under cross-polarized light; (i) metasomatic pseudomorphic texture of hornblende with 56° cleavage angle due to biotitic alteration under cross-polarized light; (j) quartz-pyrite veinlets on the edge of carbonate vein under cross-polarized light. Q-quartz, Pl-plagioclase, Bt-biotite, Hbl-hornblende, Ser-sericite, Cb-carbonate, Py-pyrite, Sph-sphalerite.

hosted in the andesite and andesitic tuff of the Duobaoshan Formation. The deposit is divided into the No. I, II and III ore zones from SW to NE (Fig. 3a). The No. I ore zone contains 37 orebodies, which are controlled by the NE-trending fractures. The No. II ore zone, which contains 93 orebodies and 23 tonnes of Au, is the most important ore zone in the deposit. The No. II orebodies are controlled by the NNE-, NW- and NWW-trending fractures (Fig. 3a), and high grade ore blocks, varying from 50 to 300 m in stretch length, and 1 to 20 m in thickness, are developed at the junctions of these fractures (Fig. 3b). Only one orebody has been so far found in the No. III ore zone, which has been subject to only minor exploration work. The orebodies in the Zhengguang Au deposit may be divided into supergene (oxidized) and primary parts, with a transitional zone (mixed ores) between them.

3.3. Characteristics of cryptoexplosive breccia

Three cryptoexplosive breccia bodies (J-1, J-2, J-3) partly mineralized are present in the No. I and II ore zones of the Zhengguang Au deposit (Gao et al., 2014a). The cryptoexplosive breccia bodies are commonly round- or dumbbell-shaped, and are zoned from the central hydrothermal cryptoexplosive breccia to a broader envelop of shatter breccias (Gao et al., 2014a). The cements of the breccias are silica, chlorite or sulfides (Fig. 6a–c). The breccias chiefly consist of andesitic tuff (Fig. 6d), andesite (Fig. 6e) and diorite fragments (Fig. 6f) in the upper part of the breccia bodies, and comprise increasing amounts of tonalite porphyry fragments exhibiting strong silicic, pyritic alteration and polymetallic mineralization at depth (Fig. 6g and h). The clasts in the cryptoexplosive breccia are relatively large and show angular shape in the outer edge of the breccia bodies, and are relatively small and of sub-angular or sub-rounded shape in the central part of the breccia bodies (Fig. 6i). The breccia bodies show an intrusive contact with andesitic tuff of the Duobaoshan Formation in the No. II ore zone (Fig. 6j). Many tonalite porphyry dykes were found at the bottom of the cryptoexplosive breccia bodies by recent drilling in the No. I ore zone, indicating that the tonalite porphyry may be genetically linked to the magmatic cryptoexplosion and even to the gold mineralization.

3.4. Ore mineralogy and mineralization styles

The oxidized and mixed ores have complex assemblages of hematite, limonite and malachite with various amounts of sulfide minerals, whereas the primary ores are composed of sulfides. Based on composition and occurrence, the primary ores can be classified into hydrothermal vein and cryptoexplosive breccia-hosted ores. The predominant hydrothermal vein ores are charac-

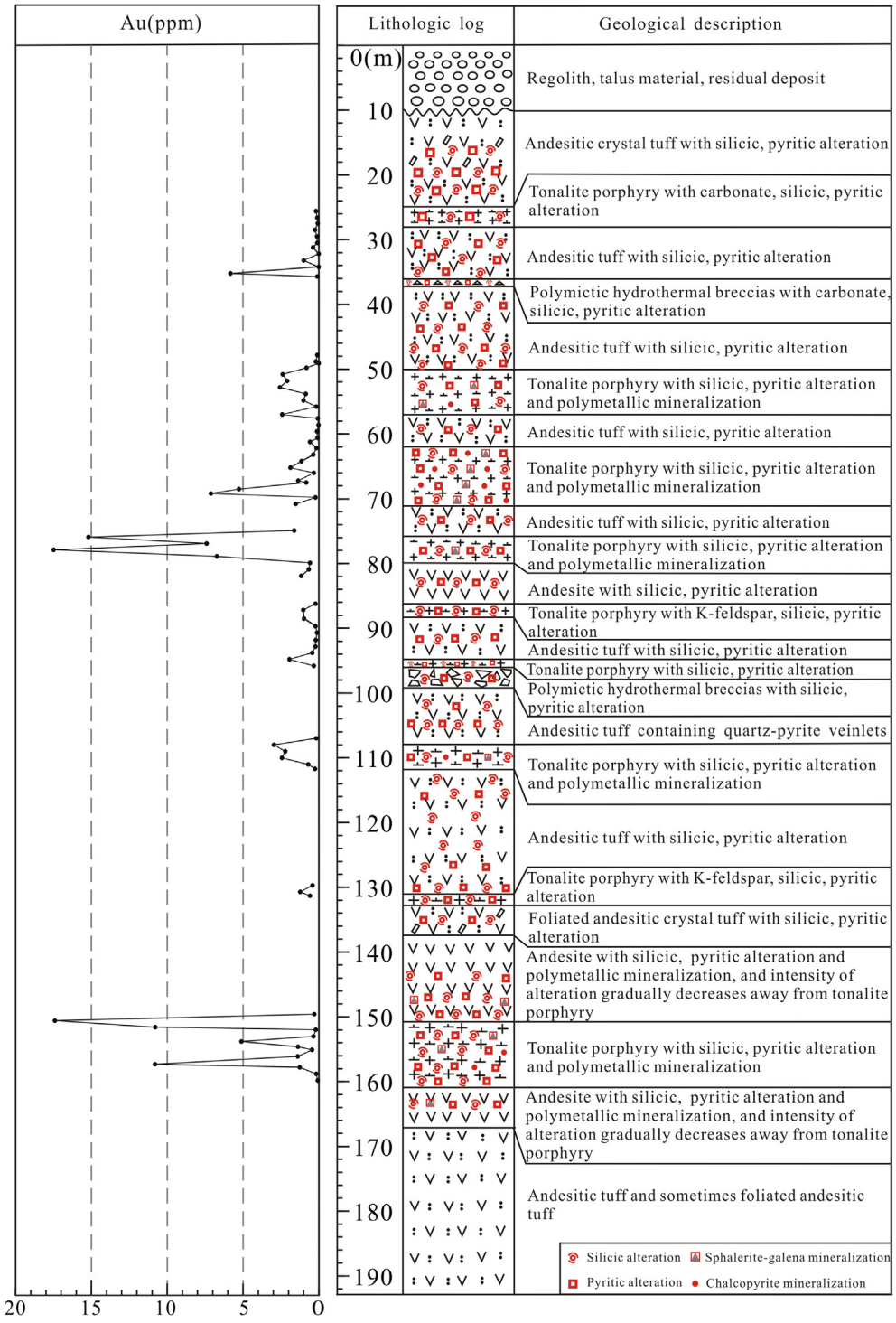

Fig. 5. Graphic log showing gold grade variation in the drill hole ZK4806 from the Zhengguang Au deposit.

terized by quartz (Fig. 7a and b) or carbonate (Fig. 7c) veins with sparely-, dense- or veinlet-disseminated sulfides including pyrite, sphalerite, galena, and chalcopyrite. Field observations indicate that quartz-pyrite-sphalerite and calcite-pyrite-sphalerite veins are crosscut by quartz-calcite veins (Fig. 7d), quartz-pyrite veins crosscut by calcite-pyrite veins (Fig. 7e), and quartz-pyrite veins crosscut by calcite veins (Fig. 7f). The breccia-hosted ores are characterized by disseminated sulfides including pyrite, chalcopyrite and bornite. The cement of the cryptoexplosive breccias (including chlorite, fine-grained magnetite and specularite) is commonly crosscut by quartz-chalcopyrite aggregations (Fig. 7g), quartz-calcite veins (Fig. 6a and c) and quartz-pyrite veins (Fig. 7h).

In these two types of sulfide ores, pyrite is the most abundant metallic mineral and generally coexists with various amounts of galena, sphalerite, bornite and chalcopyrite. There are at least three generations of pyrite including coarse crushed pyrite grains in the quartz-pyrite veins (Fig. 8a), euhedral-subhedral coarse pyrite grains with galena, sphalerite or chalcopyrite inclusions (Fig. 8b), and fine pyrite grains with a cubic shape in quartz-carbonate veins (Fig. 8c). Chalcopyrite occurs locally as droplet- or bean-shaped

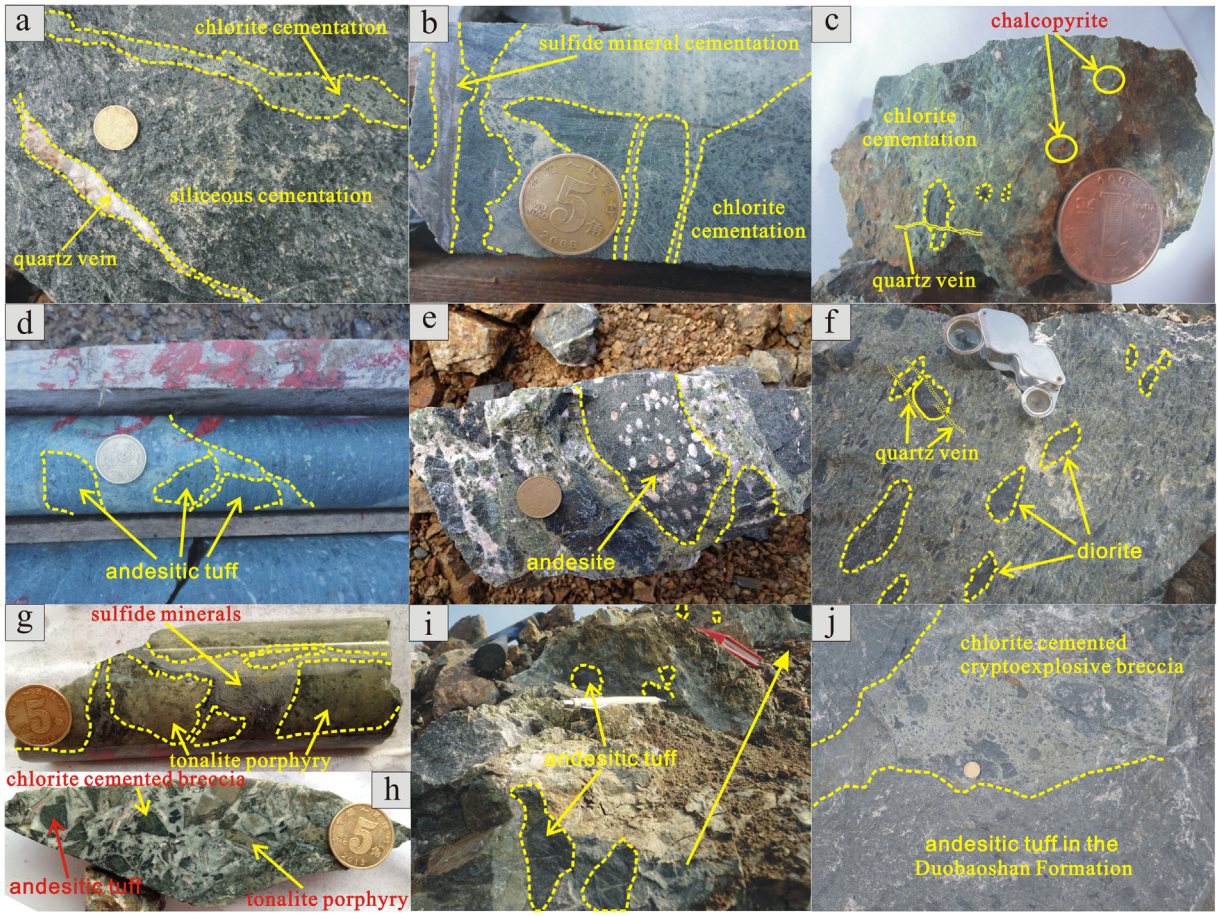

Fig. 6. Photographs of typical cryptoexplosive breccias and their geological features from the Zhengguang Au deposit. (a) siliceous cementation crosscut by chlorite cementation; (b) chlorite cementation crosscut by sulfide mineral cementation including pyrite and other sulfide minerals; (c) chlorite-cemented cryptoexplosive breccia containing disseminated chalcopyrite crosscut by a quartz vein; (d) chlorite-cemented cryptoexplosive breccia and clasts of andesitic tuff with a angular shape; (e) chlorite-cemented cryptoexplosive breccia and clasts of andesite with a sub-angular shape; (f) chlorite-cemented cryptoexplosive breccia and clasts of diorite with a sub-angular or sub-rounded shape; (g) sulfide mineral-cemented cryptoexplosive breccia and clasts of tonalite porphyry with a angular shape; (h) sulfide mineral-cemented cryptoexplosive breccia and complex clasts including the former breccias; (i) clasts become smaller and their angular shape changes to sub-angular or sub-rounded shape from outer edge to the center; (j) the intrusive contact relationship between the chlorite-cemented cryptoexplosive breccia and andesitic tuff in the Duobaoshan Formation.

grains within sphalerite due to exsolution, commonly known as chalcopyrite disease (Fig. 8b). In contrast, angular galena or chalcopyrite replaces sphalerite, occasionally resulting in the latter exhibiting embayed or isolated forms (Fig. 8b, d, e, f). A few euhedral or subhedral fine magnetite grains occur in the sphalerite grains (Fig. 8d–f), and euhedral specularite grains in the chalcopyrite grains (Fig. 8g). In places tabular specularite is crosscut by chalcopyrite (Fig. 8g). Gold mineralization is associated with sulfides, with pyrite being the principal gold-bearing sulfide mineral. Gold within pyrite may occupy cationic vacancy positions or form Au-As-S compounds (Che and Zhou, 2014). Occasionally electrum was observed in the contact zone between sphalerite and galena (Fig. 8h), as well as in the coarse-grained pyrite (Fig. 8i) of the quartz or carbonate polymetallic sulfide veins.

3.5. Wall rock alteration

Almost all the host rocks including andesite and andesitic tuff in the Duobaoshan Formation and diorite as well as tonalite porphyry are altered to some extent. The wall rock alteration can be classified as low-temperature and high-temperature, with the low-temperature alteration divided into two phases (Hao et al., 2015). The early phase is characterized by propylitic alteration containing important amounts of chlorite, epidote and carbonate minerals while the later phase is distinguished by silicic, sericitic, pyrite-sericite-quartz, kaolinite and other clay-type alteration (Fig. 3a). Gold mineralization is temporally and spatially associated with pyrite-sericite-quartz alteration (Deng et al., 2013). The bleaching distributed on one or both sides of the orebodies in the No. II ore zone was identified as representing silicic, kaolinite and illite alteration based on X-ray powder diffraction spectral analysis. High-temperature K-feldspar and biotite alteration occurs in the deep drill holes of the No. I ore zone. K-feldspar alteration characterized by variable amounts of quartz, K-feldspar and pyrite is developed in the tonalite porphyry (Fig. 4e) or volcanic rocks of the Duobaoshan Formation. Biotitic alteration is developed in the tonalite porphyry (Fig. 4i).

Recent drilling data has shown that high-temperature alteration, as well as the subsequent low-temperature alteration, are best developed in the contact zone between the Duobaoshan Formation and the tonalite porphyry block, where gold mineralization is concentrated. The intensity of alteration generally decreases away from the concealed tonalite porphyry, and the best mineralization in the Duobaoshan Formation is always associated with tonalite porphyry dykes (Fig. 5).

3.6. Paragenesis

The mineralization in the Zhengguang Au deposit is divided into the hypogene (hydrothermal) and supergene (Fig. 9). Based on

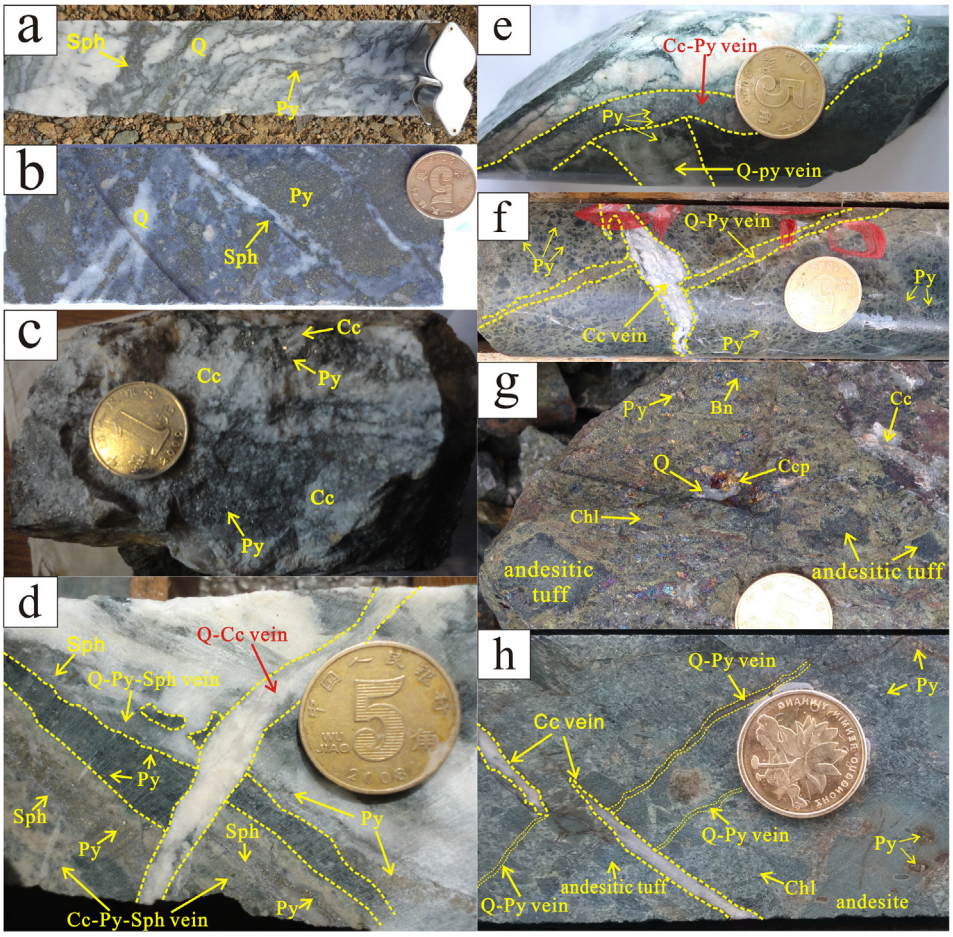

Fig. 7. Typical photographs of ore structure or ore types from the Zhengguang Au deposit. (a) veinlet-disseminated sulfides including pyrite and sphalerite in a quartz vein; (b) dense-disseminated sulfides including pyrite and sphalerite in a quartz vein; (c) disseminated sulfides including pyrite and minor galena in a calcite vein; (d) quartz-pyrite-sphalerite vein and calcite-pyrite-sphalerite vein crosscut by a quartz-calcite vein with miarolitic structure; (e) quartz-pyrite vein crosscut by a calcite-pyrite vein; (f) quartz-pyrite veins and mineralized cryptoexplosive breccia with intensive silicic and pyritic alteration crosscut by a calcite vein; (g) disseminated sulfides including pyrite, bornite, chalcopyrite in the cryptoexplosive breccia-hosted ore; (h) chlorite cement with disseminated pyrite and andesite breccia with pore-filling pyrite in the chlorite-cemented cryptoexplosive breccia, crosscut by calcite veins and quartz-pyrite veins. Q-quartz; Cc-calcite; Chl-chlorite; Py-pyrite; Sph-sphalerite; Bn-bornite; Ccp-chalcopyrite.

mineral assemblages, crosscutting relationships of the mineralized veins or veinlets, and textural characteristics of the ore minerals, five hydrothermal stages have been identified (Fig. 9): (I) chlorite-magnetite-specularite stage, (II) quartz-pyrite stage, (III) quartz-polymetallic sulfide stage, (IV) carbonate-polymetallic sulfide stage, and (V) quartz-carbonate stage. The supergene stage is characterized by hematite, limonite, and malachite.

4. Samples and analytical methods

4.1. Zircon U-Pb dating

One tonalite porphyry sample (ZG-01; ~3 kg) obtained from the drill hole ZK5808 at a depth of 630 m (Fig. 3a) was selected for zircon LA-ICPMS U-Pb dating. The sample was sent to the mineral separation laboratory of the regional geology minerals investigation research institute, Hebei province, China. Zircon grains were collected via conventional density and magnetic techniques, before being handpicked under a binocular microscope. Transmitted and reflected microscopy images were then taken in order to examine exterior structures, with cathodoluminescence (CL) images obtained to examine internal structures and to select points for U-Pb analysis. Zircon U-Pb dating analyses were conducted by LA-ICPMS at the State Key Laboratory of Geological Processes and Mineral Resources, China University of Geosciences, Wuhan. Zircon U-Th-Pb measurements were carried out under a 32 μm diameter laser beam using a GeoLas 2005 system. An Agilent 7700a ICP-MS instrument was employed to acquire ion-signal intensities with a 193 nm ArF-excimer laser and a homogenizing, imaging optical system (MicroLas, Gottingen, Germany). A detailed description of the instrumentation and its analytical accuracy can be found in Liu et al. (2008, 2010c). U-Pb dating was performed on the in-house software program ICPMSDatacal (ver 9.0, China University of Geosciences, Wuhan) (Liu et al., 2008), with Isoplot 3.0 software used to calculate ages, as well as to draw LA-ICPMS zircon U-Pb concordant diagrams and weighted average age schematic diagrams following the processing procedures described by Ludwig (2003). Errors associated with individual analyses are quoted at 1σ and those for weighted mean ages at 2σ with a 95% confidence level.

4.2. S- and Pb-isotopic analysis

Four samples (ZG-24, ZG-66, ZG-68, ZG-70) from the open pit in the No. II ore zone and two samples (ZK4607-13, ZK5807-7) from

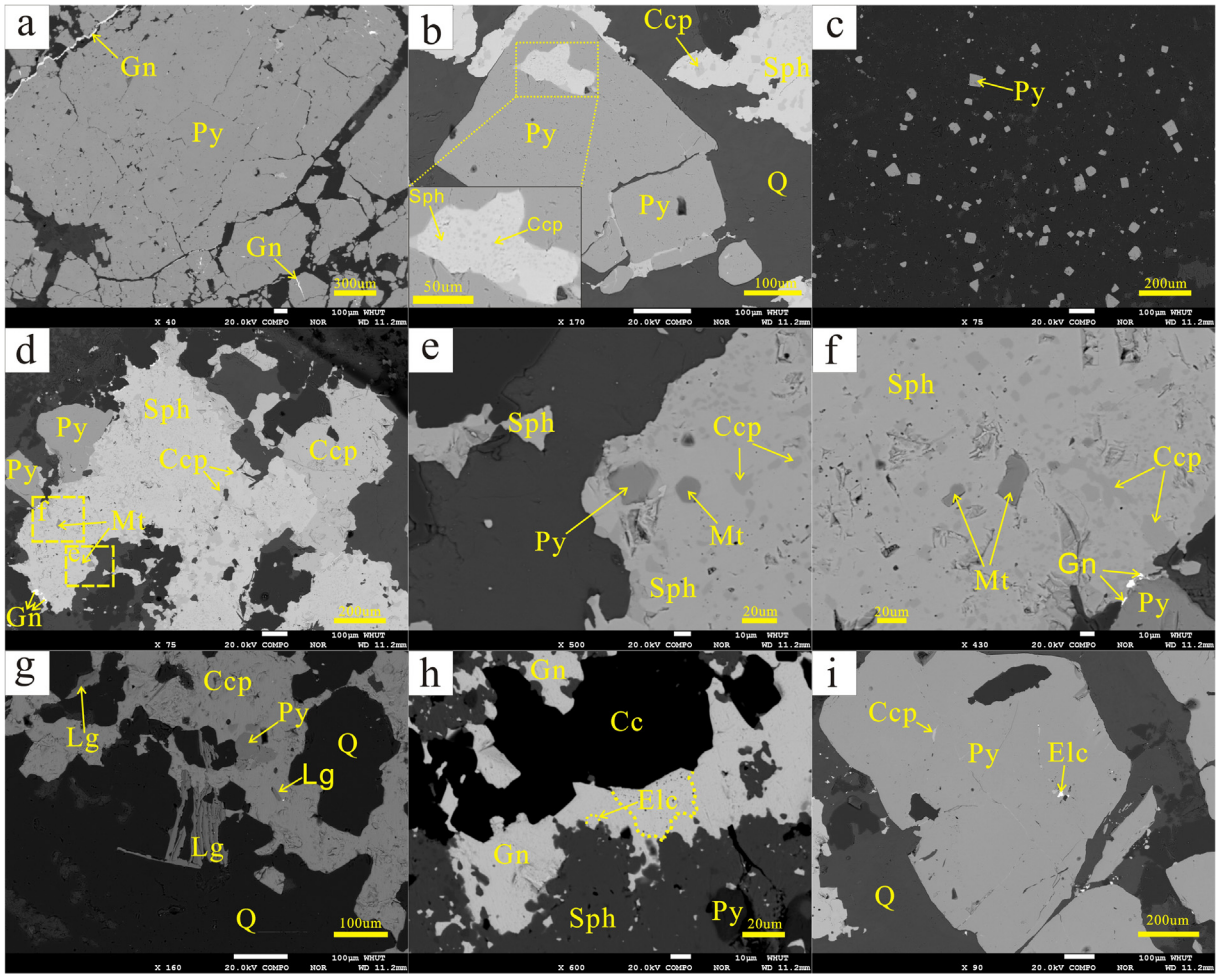

Fig. 8. Photomicrographs showing the typical textures and occurrences of gold from the Zhengguang Au deposit. (a) coarse crushed pyrite grains of the first generation and fracture-filling galena veins; (b) hypidiomorphic pyrite of the second generation with sphalerite inclusion and sphalerite containing angular- and bean-shaped chalcopyrite inclusion; (c) fine-crystallized pyrite with a cubic shape in quartz-carbonate veins; (d) sphalerite presenting harbor and isolated island shapes due to the replacement of chalcopyrite and sphalerite containing fine magnetite grains; (e) angular chalcopyrite replacing the sphalerite grains containing fine magnetite grains; (f) angular chalcopyrite replacing sphalerite grains containing fine magnetite grains; (g) plate-shaped specularite aggregates crosscut by chalcopyrite containing needle-shaped specularite; (h) electrum occurring in the contact zone between sphalerite and galena; (i) electrum occurring in coarse-grained pyrite of the quartz polymetallic sulfide veins. Py-pyrite; Sph-sphalerite; Ccp-chalcopyrite; Gn-galena; Mt-magnetite; Lg-specular hematite; Elc-electrum; Cc-calcite; Q-quartz.

drill holes in the No. I ore zone were collected for S and Pb isotopic analysis. Samples were obtained from pyrite-sericite-quartz altered andesitic tuff (ZG-66) and various different hydrothermal veins, including a quartz-pyrite vein (ZG-68), quartz-polymetallic sulfide veins (ZG-24, ZK4607-13, ZK5807-7) and carbonate-polymetallic sulfide vein (ZG-70).

Separate pyrite and galena grains were extracted from crushed material (40–60 mesh-size) and concentrated by hand-picking under a binocular microscope to a purity higher than 99%, followed by cleaning in doubly distilled water at the China University of Geosciences, Wuhan. The sulfide samples were then sent to the analytical laboratory at the Beijing Research Institute of Uranium Geology for S and Pb isotopic analysis. Sulfur in the sulfides was first converted to SO_2 by reacting with Cu_2O using a continuous flow device, and then analyzed with a Finnigan MAT-251 mass spectrometer. The accuracy of the S isotope analyses is better than ±0.2‰. Lead in the sulfides was extracted by reacting with $HF + HClO_4$ solutions, followed by ion exchange processes, and then analyzed with an ISOPROBE-T surface ionization mass spectrometer. The analytical error for 1 μg Pb is less than 0.05% for $^{206}Pb/^{204}Pb$ and less than 0.005% for $^{208}Pb/^{206}Pb$.

5. Results

5.1. Zircon U-Pb age

A total of 20 spots on 20 zircon grains from the tonalite porphyry (sample ZG-01) were analyzed by LA-ICPMS (Fig. 10a), the results of which are listed in Table 1. Zircon grains are mostly colorless or yellowish brown without any inclusions. The grains commonly occur as short columns, with a small portion exhibiting elliptical or irregular shapes ranging from 100 μm to 170 μm and length-width ratios of 1–4. Most of the zircon grains possess obvious growth zoning without a core-rim structure in the CL images (Fig. 10a). Th content is between 188 ppm and 1932 ppm, while U content is between 916 ppm and 3451 ppm. The Th/U ration varies from 0.19 to 0.56, which is much bigger than 0.1. The above information is indicative of a typically magmatic genesis for all the analyzed zircon grains. The $^{206}Pb/^{238}U$ ages of the 20 analytical points range from 458 ± 4 Ma to 467 ± 4 Ma, with a weighted mean $^{206}Pb/^{238}U$ age of 462.1 ± 1.8 Ma (n = 20, MSWD = 0.34) and a concordia age of 462.0 ± 0.9 Ma (n = 20, MSWD = 0.0025) in the U-Pb concordant diagrams (Fig. 10b). The weighted mean age is interpreted to be the crystallization age of the tonalite porphyry.

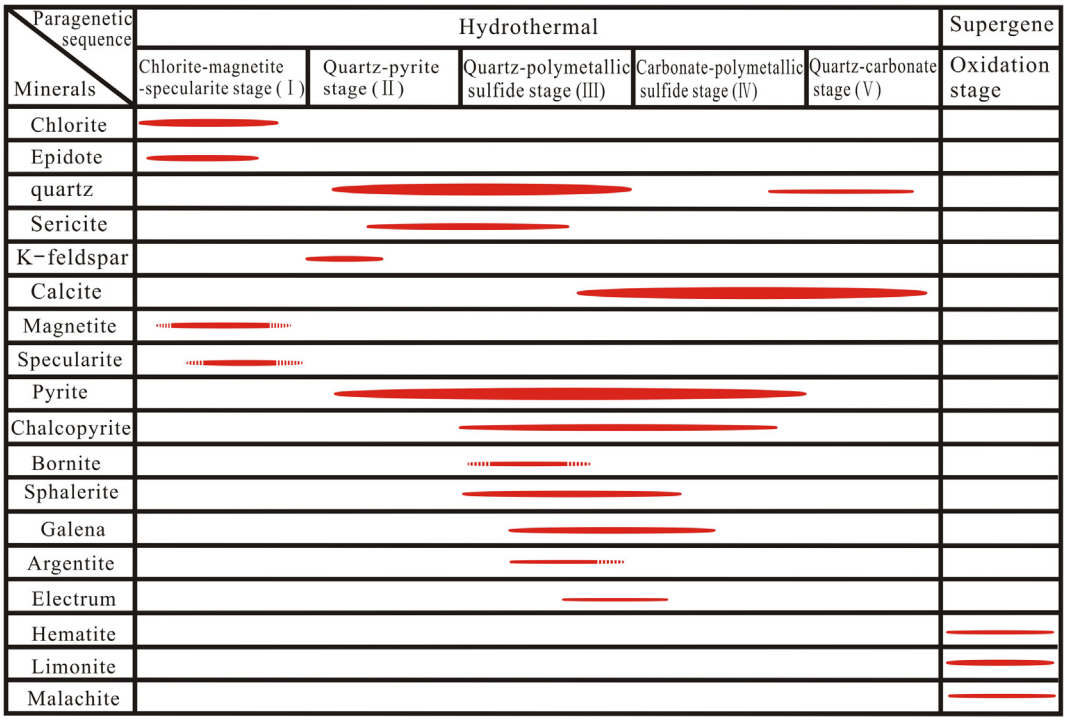

Fig. 9. Paragenetic sequence of ore and gangue minerals from the Zhengguang Au deposit.

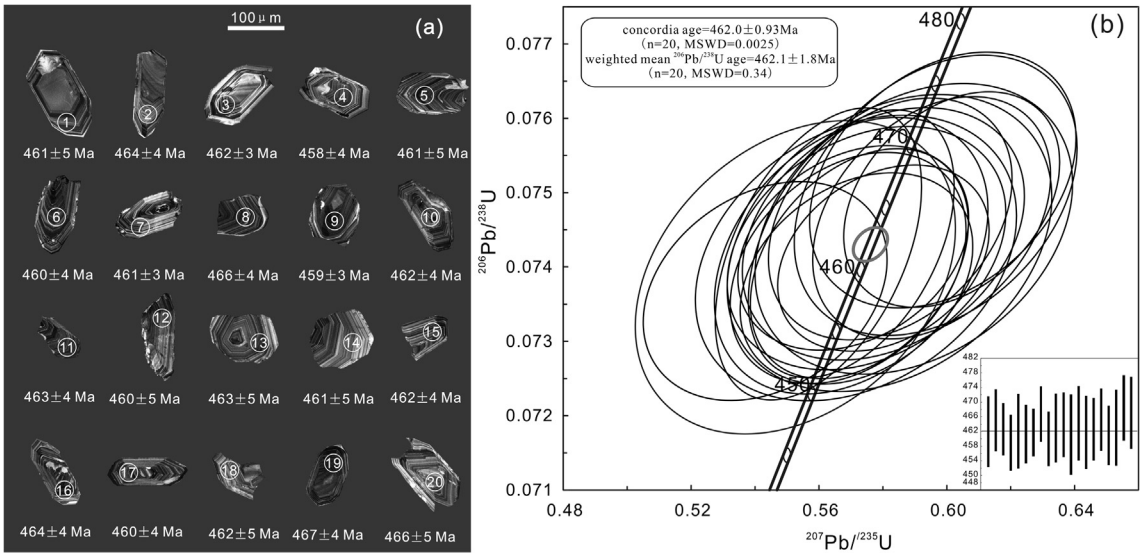

Fig. 10. Cathodoluminescence (CL) images of zircons and U-Pb dating analytical points (a); zircon U-Pb concordant diagrams and weighted average age schematic diagram (b) for the tonalite porphyry from the Zhengguang Au deposit.

5.2. S isotope geochemistry

The S isotopic compositions of 28 samples obtained from the Zhengguang gold deposit during both this study and previous studies are listed in Table 2. In this study, the $\delta^{34}S_{V\text{-}CDT}$ values of sulfides vary narrowly from −3.0‰ to −1.7‰, with an average of −2.33‰. One galena sample yielded a $\delta^{34}S_{V\text{-}CDT}$ value of −1.7‰ and five pyrite samples consistent values of −3.0‰ to −1.8‰. Although these $\delta^{34}S_{V\text{-}CDT}$ values are similar to those ($\delta^{34}S_{V\text{-}CDT}$ values of ten pyrite samples ranging from −2.9‰ to 0.7‰, and of two sphalerite samples between −1.5‰ and −1.7‰) measured by Ma. (1984), they differ from the results ($\delta^{34}S_{V\text{-}CDT}$ values of ten pyrite samples ranging from −15‰ to −1.5‰) recorded by Fu et al. (2014).

5.3. Pb isotope geochemistry

The Pb isotopic compositions of pyrite in the ores, Duobaoshan Formation and diorite from the Zhengguang gold deposit during both this study and previous studies are presented in Table 3. In the pyrite samples, the ratios of $^{206}Pb/^{204}Pb$ vary from 17.572 to 17.629 with an average of 17.600, the ratios of $^{207}Pb/^{204}Pb$ from 15.424 to 15.486 with an average of 15.449, and the ratios of $^{208}Pb/^{204}Pb$ from 37.206 to 37.418 with an average of 37.292.

Table 1
LA-ICPMS U-Pb data of zircon grains for the tonalite porphyry from the Zhengguang gold deposit.

Points	Content(ppm)			Ratios									(Ma)	
	Th	U	Pb	Th/U	$^{207}Pb/^{206}Pb$	1σ	$^{207}Pb/^{235}U$	1σ	$^{206}Pb/^{238}U$	1σ	$^{208}Pb/^{232}Th$	1σ	$^{207}Pb/^{235}U$	$^{206}Pb/^{238}U$
ZG-01-01	446	1799	252	0.25	0.0554	0.00172	0.5701	0.01748	0.0742	0.00076	0.0244	0.00082	458 ± 11	461 ± 5
ZG-01-02	632	2046	326	0.31	0.0561	0.00146	0.5823	0.01557	0.0746	0.00066	0.0231	0.00067	466 ± 10	464 ± 4
ZG-01-03	1501	2912	654	0.52	0.0553	0.00140	0.5707	0.01475	0.0743	0.00056	0.0231	0.00056	458 ± 10	462 ± 3
ZG-01-04	394	1564	222	0.25	0.0532	0.00153	0.5432	0.01559	0.0737	0.00060	0.0234	0.00070	441 ± 10	458 ± 4
ZG-01-05	409	1636	229	0.25	0.0545	0.00128	0.5598	0.01319	0.0742	0.00080	0.0231	0.00062	451 ± 9	461 ± 5
ZG-01-06	536	1732	276	0.31	0.0557	0.00134	0.5726	0.01394	0.0740	0.00063	0.0222	0.00050	460 ± 9	460 ± 4
ZG-01-07	534	1780	288	0.30	0.0562	0.00125	0.5802	0.01352	0.0741	0.00051	0.0223	0.00047	465 ± 9	461 ± 3
ZG-01-08	602	1946	329	0.31	0.0579	0.00136	0.6015	0.01380	0.0749	0.00059	0.0221	0.00043	478 ± 9	466 ± 4
ZG-01-09	334	1590	209	0.21	0.0559	0.00149	0.5717	0.01487	0.0738	0.00058	0.0226	0.00066	459 ± 10	459 ± 3
ZG-01-10	1619	3100	710	0.52	0.0552	0.00119	0.5701	0.01316	0.0743	0.00074	0.0214	0.00043	458 ± 9	462 ± 4
ZG-01-11	393	1336	218	0.29	0.0561	0.00171	0.5802	0.01803	0.0744	0.00069	0.0230	0.00068	465 ± 12	463 ± 4
ZG-01-12	188	916	120	0.21	0.0541	0.00205	0.5528	0.02046	0.0740	0.00086	0.0231	0.00086	447 ± 13	460 ± 5
ZG-01-13	277	1278	171	0.22	0.0570	0.00196	0.5897	0.02029	0.0745	0.00080	0.0232	0.00092	471 ± 13	463 ± 5
ZG-01-14	194	1009	124	0.19	0.0557	0.00205	0.5716	0.02052	0.0741	0.00078	0.0226	0.00097	459 ± 13	461 ± 5
ZG-01-15	863	2184	401	0.40	0.0558	0.00175	0.5749	0.01780	0.0743	0.00067	0.0219	0.00057	461 ± 11	462 ± 4
ZG-01-16	1932	3451	835	0.56	0.0574	0.00145	0.5953	0.01520	0.0747	0.00067	0.0226	0.00053	474 ± 10	464 ± 4
ZG-01-17	1197	2782	540	0.43	0.0554	0.00147	0.5691	0.01508	0.0740	0.00064	0.0218	0.00053	457 ± 10	460 ± 4
ZG-01-18	334	1467	188	0.23	0.0566	0.00206	0.5821	0.02075	0.0743	0.00082	0.0225	0.00077	466 ± 13	462 ± 5
ZG-01-19	768	2438	397	0.32	0.0574	0.00164	0.5987	0.01703	0.0752	0.00070	0.0236	0.00064	476 ± 11	467 ± 4
ZG-01-20	477	1818	262	0.26	0.0572	0.00168	0.5965	0.01807	0.0750	0.00077	0.0235	0.00068	475 ± 11	466 ± 5

Table 2
S-isotopic compositions of sulfide minerals from the Zhengguang gold deposit.

Sample No.	Occurrences and location	Mineral	$\delta^{34}S_{V\text{-}CDT}$ ‰	Sources
ZG-66	Pyrite-sericite-quartz altered andesitic tuff	Pyrite	−2.4	This study
ZG-68	Ore: quartz-pyrite vein	Pyrite	−1.8	This study
ZK5807-7	Ore: quartz-poly-metallic sulfide vein	Pyrite	−2.6	This study
ZK4607-13	Ore: quartz-poly-metallic sulfide vein	Pyrite	−2.5	This study
ZG-24	Ore: quartz-poly-metallic sulfide vein	Galena	−1.7	This study
ZG-70	Ore: carbonate-poly-metallic sulfide vein	Pyrite	−3.0	This study
205-5-2	Ore: carbonate-poly-metallic sulfide vein	Pyrite	−4.4	Fu et al. (2014)
205-8	Ore: carbonate-poly-metallic sulfide vein	Pyrite	−2.4	Fu et al. (2014)
205-9	Ore: quartz-pyrite vein	Pyrite	−12.1	Fu et al. (2014)
205-10	Ore: quartz-pyrite vein	Pyrite	−4.1	Fu et al. (2014)
205-11	Ore: quartz-pyrite vein	Pyrite	−5.4	Fu et al. (2014)
205-12	Ore: quartz-pyrite vein	Pyrite	−8.9	Fu et al. (2014)
205-21-1	Ore: carbonate-poly-metallic sulfide vein	Pyrite	−3.2	Fu et al. (2014)
205-27	Ore: quartz-pyrite vein	Pyrite	−3.9	Fu et al. (2014)
60-4-6	Ore: carbonate-poly-metallic sulfide vein	Pyrite	−1.5	Fu et al. (2014)
046-7	Ore: quartz-poly-metallic sulfide vein	Pyrite	−1.9	Fu et al. (2014)
Unknown	Ore	Sphalerite	−1.5	Ma (1984)
Unknown	Ore	Sphalerite	−1.7	Ma (1984)
Unknown	Ore (ten ore samples)	Pyrite	−2.7–0.9	Ma (1984)

Table 3
Pb-isotopic compositions of sulfide minerals, diorite and andesitic tuff in the Duobaoshan Formation from the Zhengguang gold deposit.

Sample No.	Occurrences and location	Mineral/rock	$^{206}Pb/^{204}Pb$	$^{207}Pb/^{204}Pb$	$^{208}Pb/^{204}Pb$	Sources
ZG-66	Pyrite-sericite-quartz altered andesitic tuff	Pyrite	17.573	15.432	37.231	This study
ZG-68	Ore: quartz-pyrite vein	Pyrite	17.572	15.424	37.206	This study
ZK4607-13	Ore: quartz-poly-metallic sulfide vein	Pyrite	17.614	15.433	37.247	This study
ZK5807-7	Ore: quartz-poly-metallic sulfide vein	Pyrite	17.629	15.486	37.418	This study
ZG-70	Ore: carbonate-poly-metallic sulfide vein	Pyrite	17.614	15.471	37.36	This study
6093	Diorite	Whole rock	17.855	15.148	36.617	Zheng (2012)
6094	Duobaoshan Formation: andesitic tuff	Whole rock	17.635	15.484	37.36	Zheng (2012)
6098	Duobaoshan Formation: andesitic tuff	Whole rock	18.055	15.439	37.346	Zheng (2012)
6099	Duobaoshan Formation: andesitic tuff	Whole rock	18.392	15.586	37.697	Zheng (2012)
6102	Duobaoshan Formation: andesitic tuff	Whole rock	17.676	15.438	37.264	Zheng (2012)

Whole rock analysis of the Duobaoshan Formation samples revealed the ratios of $^{206}Pb/^{204}Pb$ ranging from 17.635 to 18.392 with an average of 17.940, the ratios of $^{207}Pb/^{204}Pb$ from 15.148 to 15.586 with an average of 15.487, and the ratios of $^{208}Pb/^{204}Pb$ from 36.617 to 37.697 with an average of 37.417. Whole rock analysis of the diorite sample produced that the ratios of $^{206}Pb/^{204}Pb$, $^{207}Pb/^{204}Pb$, $^{208}Pb/^{204}Pb$ are 17.855, 15.148 and 36.617, respectively.

In the $^{207}Pb/^{206}Pb$-$^{206}Pb/^{204}Pb$ diagram shown in Fig. 11a, the pyrite samples lie close to the evolution curve of mantle, and the Duobaoshan Formation samples fall between the evolution curves of mantle and upper crust (Zartman and Doe, 1981). In contrast, the diorite sample is located far from both the pyrite and Duobaoshan Formation samples, falling below the evolution curve of upper crust (Zartman and Doe, 1981). Similarly, in the $^{208}Pb/^{206}Pb$-$^{206}Pb/^{204}Pb$ diagram shown in Fig. 11b, the pyrite sam-

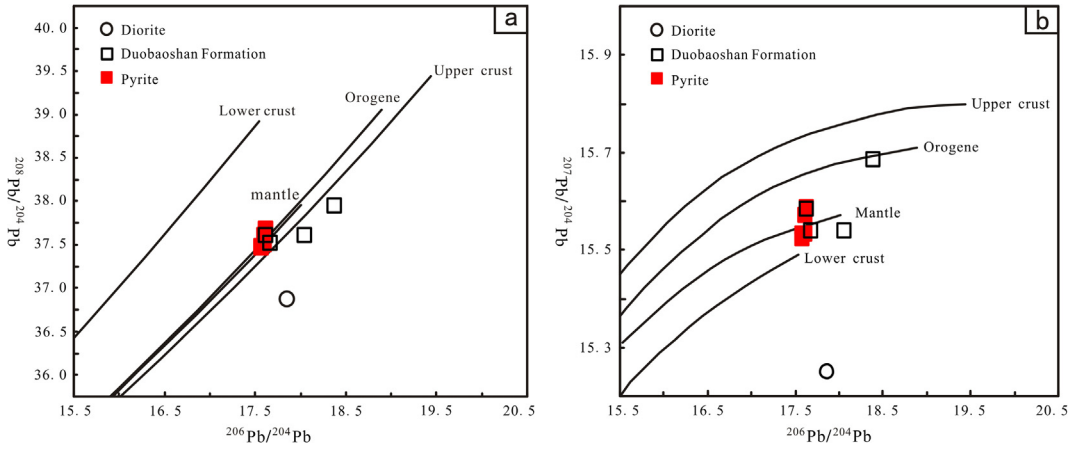

Fig. 11. Pb isotopic compositions of sulfide minerals, Duobaoshan Formation and diorite from the Zhengguang Au deposit. The evolution lines for the mantle, orogene, upper crust and lower crust are from Zartman and Doe (1981). (a) $^{207}Pb/^{206}Pb$-$^{206}Pb/^{204}Pb$ diagram; (b) $^{208}Pb/^{206}Pb$-$^{206}Pb/^{204}Pb$ diagram.

ples lie close to the evolution curve of mantle, and the Duobaoshan Formation samples fall between the evolution curves of mantle and orogene (Zartman and Doe, 1981). The diorite sample is again far from the pyrite and Duobaoshan Formation samples, falling below the evolution curve of lower crust (Zartman and Doe, 1981).

6. Discussion

6.1. Age of mineralization and related magmatism

Although many geochronological studies targeting the Duobaoshan and Tongshan Cu-Mo deposits in the Duobaoshan ore field have been reported (Zhao et al., 1997; Wang et al., 2007; Ge et al., 2007; Han et al., 2007; Li, 2011; Zhao et al., 2011; Zeng et al., 2014; Hao et al., 2015; Liu et al., 2015; Hu et al., 2016), as summarized in Table 4, the age of mineralization and related magmatism in the Zhengguang Au deposit remain uncertain. Wu et al. (2006), Fu and Yang (2010), and Zheng (2012) believe that the diorite is closely related to the gold mineralization, and therefore the crystallization age approximately corresponds to the mineralization age. A nearby quartz diorite with similar petrological characteristics as the diorite in the deposit area has a zircon U-Pb age of 186 Ma (Zheng, 2012), and therefore the Zhengguang Au deposit was thought to have formed by early Jurassic magmatism. More recent zircon U-Pb dating of mineralized diorite yielded a weighted mean $^{206}Pb/^{238}U$ age of 480.7 ± 3.2 Ma (Shen et al., 2014) and three zircon U-Pb ages of 538.1 ± 2.4 Ma, 494.34 ± 0.99 Ma and 459.7 ± 1.4 Ma (Fu et al., 2014). Re-Os isotopic dating of molybdenite collected from a drill hole on the periphery of the Zhengguang ore district yielded an isochron age of 462 ± 24 Ma (Li et al., 2016), indicating that the Zhengguang Au deposit may be a product of Ordovician mineralization.

Based on the characteristics of cryptoexplosive breccia and hydrothermal alteration indicative of porphyry-type and epithermal mineralization, we proposed that the tonalite porphyry, rather than the pre-mineral dorite, has a genetic relationship with gold mineralization. Considering that zircon U-Pb isotope dating is the most precise method for geochronological study, the tonalite porphyry provides an ideal opportunity to constrain the mineralization age. The zircon LA-ICPMS U-Pb age of 462.1 ± 1.8 Ma obtained in this study is consistent with the molybdenite Re-Os

Table 4
Geochronological ages from the Duobaoshan Cu-Mo deposit, Tongshan Cu-Mo deposit and Zhengguang Au deposit.

Rock/ore	Location	Measuring sample	Method	Age(Ma)	Sources
Granodiorite porphyry	Duobaoshan Cu-Mo deposit	Zircon	LA-ICPMS U-Pb	477.2 ± 4.0	Zeng et al. (2014)
Granodiorite porphyry	Duobaoshan Cu-Mo deposit	Zircon	LA-ICPMS U-Pb	474.8 ± 4.7	Xiang et al. (2012)
Granodiorite	Duobaoshan Cu-Mo deposit	Zircon	LA-ICPMS U-Pb	481.5 ± 3.7	Zeng et al. (2014)
Granodiorite	Duobaoshan Cu-Mo deposit	Zircon	SHRIMP U-Pb	479.5 ± 4.6	Cui et al. (2008)
Granodiorite	Duobaoshan Cu-Mo deposit	Zircon	SHRIMP U-Pb	485 ± 8	Ge et al. (2007)
Granodiorite	Duobaoshan Cu-Mo deposit	Zircon	LA-ICPMS U-Pb	478.1 ± 4.1	Xiang et al. (2012)
Ore	Duobaoshan Cu-Mo deposit	Molybdenite	Re-Os	475.1 ± 5.1	Xiang et al. (2012)
Ore	Duobaoshan Cu-Mo deposit	Molybdenite	Re-Os	507–521	Zhao et al. (1997)
Ore	Tongshan Cu-Mo deposit	Molybdenite	Re-Os	476–505	Zhao et al. (1997)
Ore	Duobaoshan Cu-Mo deposit	Molybdenite	Re-Os	476–480	Zeng et al. (2014)
Ore	Duobaoshan Cu-Mo deposit	Chalcopyrite	Re-Os	477–489	Liu et al. (2012b)
Ore	Duobaoshan Cu-Mo deposit	Pyrite	Re-Os	483–487	Liu et al. (2012b)
Ore	Duobaoshan Cu-Mo deposit	Molybdenite	Re-Os	485.6 ± 3.7	Liu et al. (2012b)
Granodiorite	Tongshan Cu-Mo deposit	Zircon	LA-ICPMS U-Pb	475.9 ± 0.8	Hao et al. (2015)
Granodiorite	Tongshan Cu-Mo deposit	Zircon	LA-ICPMS U-Pb	478 ± 3	Hu et al. (2016)
Tonalite	Tongshan Cu-Mo deposit	Zircon	LA-ICPMS U-Pb	214 ± 3	Hu et al. (2016)
Tonalite	Tongshan Cu-Mo deposit	Zircon	LA-ICPMS U-Pb	461 ± 1	Liu et al. (2015)
Ore	Tongshan Cu-Mo deposit	Molybdenite	Re-Os	471–475	Hao et al. (2015)
Diorite	Zhengguang Au deposit	Zircon	LA-ICPMS U-Pb	480.7 ± 3.2	Shen et al. (2014)
Diorite	Zhengguang Au deposit	Zircon	LA-ICPMS U-Pb	460–538	Fu et al. (2014)
Diorite porphyry	Zhengguang Au deposit	Zircon	LA-ICPMS U-Pb	478.3 ± 3.7	Li et al. (2016)
Ore	Zhengguang Au deposit	Molybdenite	Re-Os	462 ± 24	Li et al. (2016)
Tonalite porphyry	Zhengguang Au deposit	Zircon	LA-ICPMS U-Pb	462.1 ± 1.8	This study

age of 462 ± 24 Ma (Li et al., 2016), as it has been shown that mineralization in magmatic-hydrothermal systems is generally concurrent or slightly (by several million years) later than the emplacement of the genetically related intrusions (Reynolds et al., 1998; Selby and Creaser, 2001; Mao et al., 2008). Therefore, our new chronological data confirm that the mineralization age of the Zhengguang Au deposit took place in Middle Ordovician, at ca. 462 Ma. This age, together with recent U-Pb and Re-Os ages of 470–480 Ma estimated for the Duobaoshan and Tongshan Cu-Mo deposits (Zhao et al., 1997; Ge et al., 2007; Cui et al., 2008; Liu et al., 2012; Zeng et al., 2014; Hao et al., 2015), suggests that the Zhengguang Au deposit is part of the Ordovician Duobaoshan porphyry-epithermal ore system.

6.2. Sources of metals and sulfur

The Duobaoshan Formation was traditionally considered as the main source of metals and sulfur, based on the high abundance of ore elements and presence of sulfide in the Duobaoshan ore field (Fu and Yang, 2010; Wu et al., 2006; Han et al., 2007). Furthermore, as the diorite in the Zhengguang Au deposit also has a high content of ore elements, previous researchers thought that the ore-forming materials also originated from the diorite intrusions (Wu et al., 2006; Fu and Yang, 2010). However, such a viewpoint lacks direct isotopic evidence.

The narrow ranges of Pb isotope in the analyzed pyrite samples (Table 3) at different mineralizing stages and in pyrite-sericite-quartz altered andesitic tuff from the Zhengguang Au deposit indicates that the metals may be derived from a single source. Based on their Pb isotopic compositions (Fig. 10), the pyrite samples are clearly different from the diorite, revealing that the diorite is likely not the main source of metals. The Pb isotopic data of the Duobaoshan Formation and pyrite samples are largely different but partly overlap, which suggests that the Duobaoshan Formation may have provided minor metals for mineralization. The Pb isotopic compositions of the pyrite are close to the evolution curve of mantle, indicating that the source of Pb and by inference the ore metals are predominantly derived from mantle. This inference is also consistent with a mantle source of hydrothermal fluids through use of C-O isotope geochemistry (Fu et al., 2014).

The narrow range of $\delta^{34}S$ values of pyrite and galena (from −1.7‰ to −3‰, with an average of −2.33‰) obtained in this study (Table 2), suggest that the sulfur in these minerals may be mainly derived from mantle source, perhaps through a deep seated magmatic chamber. Some relatively low values (as low as −12.1‰) reported by Fu et al. (2014) may be partly due to sulfur isotope fraction during the hydrolysis of magmatic SO_2 and fluid oxidation with decreasing temperature (Rye, 1993). Another possible reason for the discrepancy between the two studies is that some pyrite samples in the Duobaoshan Formation obtained by Fu et al. (2014) may have a sedimentary origin (Fig. 12).

Similar inferences of metal and sulfur sources can also be made for the Duobaoshan and Tongshan Cu-Mo deposits. The Duobaoshan Formation was initially regarded as the main sources of metals (Zhao and Zhang, 1997; Wang et al., 2007; Liu et al., 2010a), but more recent isotopic data suggest the ore-forming materials were derived from the magmatic intrusions. New Re-Os isotope data of molybdenite show Re contents ranging from 290.9 ppm to 729.4 ppm for the Duobaoshan Cu-Mo deposit (Zhao et al., 1997; Xiang et al., 2012; Zeng et al., 2014), and from 155.0 ppm to 1651 ppm for the Tongshan Cu-Mo deposit (Hao et al., 2015), indicating a dominant mantle origin of the metals. The $\delta^{34}S$ values of sulfides of the Duobaoshan (−5.2‰ – 3.3‰, Feng, 2008) and Tongshan (−1.3‰ – −0.4‰, Liu et al., 2015; −2.6‰ – 1.1‰, Hu et al., 2016) Cu-Mo deposits also suggest a dominant magmatic source for sulfur. Therefore, like the geochronological data, the Pb and S isotopic data also support the notion that the Zhengguang Au deposit is part of the Duobaoshan porphyry-epithermal mineralization system.

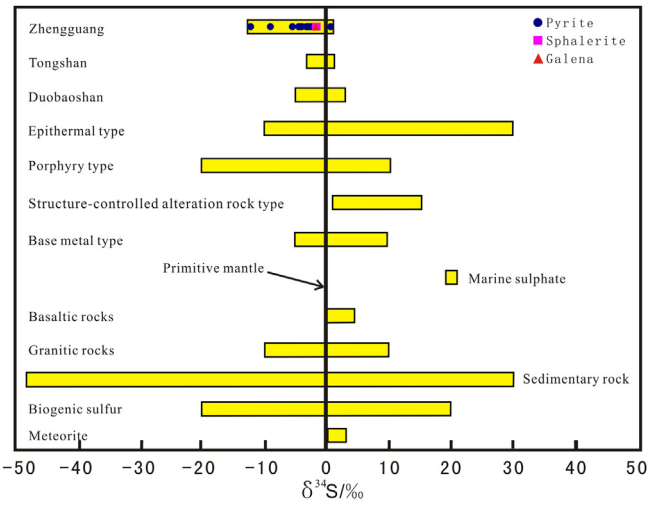

Fig. 12. $\delta^{34}S$ values of selected geologically important sulfur reservoirs (after Hoefs, 1997), the Zhengguang Au deposit, Duobaoshan Cu-Mo deposit (after Fu et al., 2014), and Tongshan Cu-Mo deposit (after Fu et al., 2014).

6.3. Mineralization model

The regional mineralization in the Duobaoshan ore field was formed in an island arc related to the subduction of the Paleo-Asian Ocean during the Ordovician, similar to the island arc in the SW Pacific that contains a large amount of porphyry as well as epithermal deposits (Ren et al., 1997; Li, 1998; Wu et al., 2011; Zeng et al., 2014). Indeed, tectono-magmatic activities during the Ordovician created favorable conditions for the porphyry-epithermal ore system. Epithermal Au mineral systems are generally developed above or laterally offset from porphyry Cu(Mo) systems, with a gradual upward and outward decrease in the proportion of magmatic components in the ore-forming fluids, as well as temperatures and salinities (Sillitoe, 2010; Richards, 2011). The gold mineralized outcrops with intensive pyrite-sericite-quartz alteration were found at the top of the Tongshan porphyry Cu-Mo deposit (Fig. 13; Li et al., 2016), representing the upper part of porphyry Cu(Mo) system overprinted by epithermal gold mineralization. The gold placers found in the drainage systems of the Duobaoshan ore field also seem to be the product of epithermal gold mineralization (Fig. 13). Therefore, the Ordovician ore-forming system in the Duobaoshan ore field may consist of porphyry and epithermal stages.

The Zhengguang Au deposit was regarded as an epithermal type deposit (Zhang, 2004; Fu and Yang, 2010; Deng et al., 2013; Song et al., 2015; Shen et al., 2014), largely because the fluid inclusion data (homogenization temperature: 130–220 °C; salinities: 0.3–10.4% $NaCl_{eqv}$; Deng et al., 2013; Gao et al., 2014b), iron-poor sphalerite (Fe content: 0.1–2.6%; Song et al., 2015) and fineness of the gold (722–729) are together indicative of low temperatures and low salinities. However, the deposit has several prominent features that differ from typical epithermal deposits as discussed below. (a) Some mineralization is hosted above the concealed tonalite porphyry that is interpreted to be related to mineralization, which is typical of epithermal deposits, but some mineralization, in the form of veinlets and dissemination, is located at the contact zone or even overprints the tonalite porphyry, which is similar to porphyry-type deposits. (b) Although the zonal pyrite-sericite-quartz and propylitic alteration is mainly of epithermal nature at

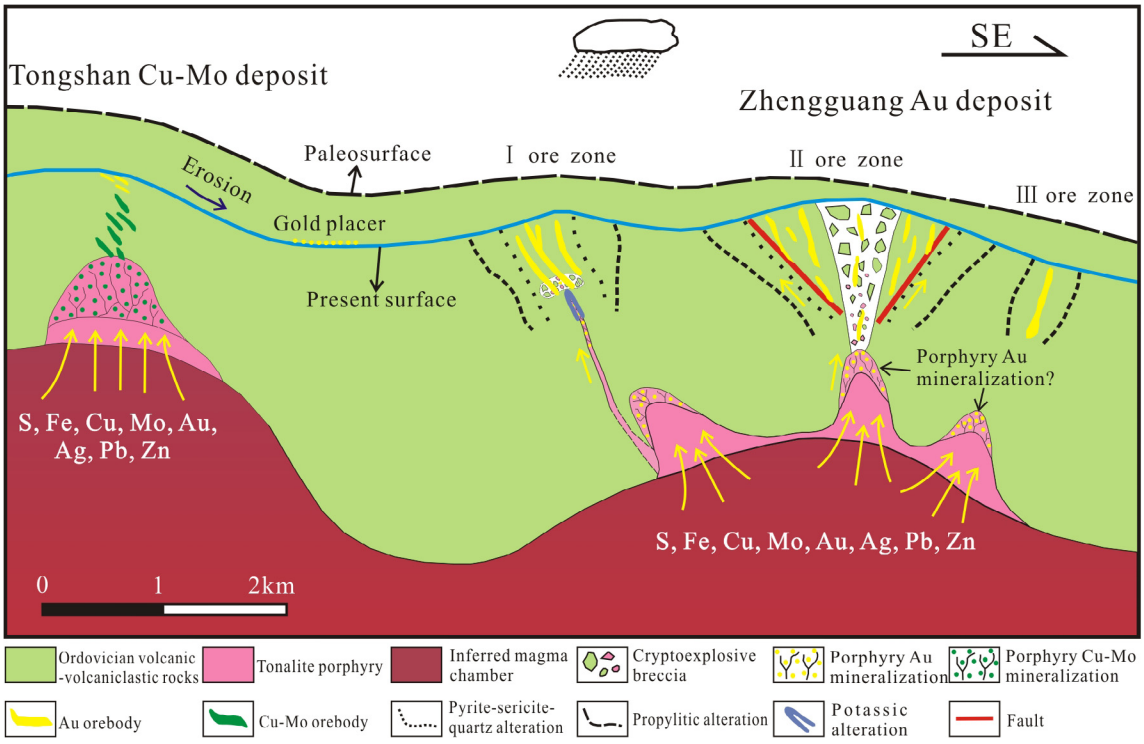

Fig. 13. Proposed genetic model for the Zhengguang Au deposit in the Duobaoshan ore field.

the surface, potassic alteration in the deep drill holes, as well as the bleaching containing kaolinite and illite alteration adjacent to the orebodies, suggest that there may be a hidden porphyry Cu(Mo)-Au system underneath. (c) The cryptoexplosive breccia-hosted ores with disseminated sulfides including pyrite, bornite and chalcopyrite contains large amounts of magnetite and specularite, which are not typically found in epithermal systems. (d) The content of sulfides in gold-bearing veinlets is generally >10%, which is much higher than 5% expected for low-sulfidation epithermal deposits as assigned by Song et al. (2015). The content of chalcopyrite gradually increases with depth in the drill holes of the No. I and II ore zones (Song et al., 2015), which is also different from what is expected for typical epithermal deposits. (e) To date, the characteristic minerals of low-sulfidation and high-sulfidation epithermal subtypes, such as adularia, alunite and enargite, have never been reported.

Based on the above discussion, we therefore propose that the Zhengguang gold deposit was formed in a porphyry to epithermal transitional environment associated with the concealed tonalite porphyry, which may be part of the Duobaoshan porphyry-epithermal ore system. During the emplacement of the tonalite porphyry, hydrothermal fluids enriched in ore-forming elements were released and accumulated above the tonalite porphyry intrusions. When the increasing pressure of the fluids was greater than that of the overlying Duobaoshan Formation, cryptoexplosion took place. Chlorite, epidote, magnetite and specularite were quickly formed in the process of the cryptoexplosion, and a large amount of reduced sulfur was released at the same time (Liang et al., 2009; Sun et al., 2004, 2013, 2015). Following this early mineralization event, the quartz-pyrite, quartz-polymetallic sulfide, carbonate-polymetallic sulfide and quartz-carbonate veins were sequentially formed with decreasing of temperature and pressure of ore-forming fluids. The veinlet-dissemination sulfide mineralization, similar to porphyry gold mineralization, occurred in the tonalite porphyry stocks or dykes and cryptoexplosive breccia bodies, while the hydrothermal vein-type mineralization occurred in the andesitic tuff and andesite of the Duobaoshan Formation as the hydrothermal fluids ascended the main faults and fractures (Fig. 13). Potassic alteration also gradually changed to pyrite-sericite-quartz and propylitic alteration with the flowing of hydrothermal fluids from deep to shallow parts of the system (Fig. 13).

7. Conclusions

(1) The mineralization in the Zhengguang gold deposit has a genetic relationship with the concealed tonalite porphyry, rather than the diorite. Zircon LA-ICPMS U-Pb dating reveals that the tonalite porphyry was emplaced at 462.1 ± 1.8 Ma (Middle Ordovician).
(2) S isotopic compositions indicate that sulfur was mainly derived from a magmatic source, and Pb isotopic compositions reveal a major mantle component for the source of the Pb and, by inference, of other ore metals. We therefore suggest that the ore-forming elements were derived from the mantle-sourced tonalite porphyry.
(3) The Zhengguang gold deposit was formed in a porphyry to epithermal transition environment associated with the concealed tonalite porphyry, which may be part of the Duobaoshan porphyry-epithermal ore system that was formed by the subduction of the Paleo-Asian Ocean during the Ordovician. The present study has provided new evidence for Ordovician gold mineralization in the Duobaoshan ore field.

Acknowledgements

We would like to thank the managers of the Heilong Mining Corporation for their support of our fieldwork. We are also deeply grateful to anonymous reviewers for their reviews and construc-

tive suggestions, and to Prof. Franco Pirajno for his editorial handling. Appreciation is expressed to Prof. Chi Guoxiang from University of Regina for his helpful comments on the paper revision. This study was supported by the Inner Mongolia Geological Exploration Foundation (Grant NO. NMKD2010-3).

References

Bai, L.A., 2013. Study on Metallogenic Mechanism and Resource Forecast of Hydrothermal Cu Deposits in the Central and North of the Greater Xing'an Mountains, NE China (PhD Thesis). Jilin University, Changchun, pp. 1–145 (in Chinese with English abstract).

Bai, L.A., Sun, J.G., Gu, A.L., Zhao, K.Q., Sun, Q.L., 2014. A review of the genesis, geochronology, and geological significance of hydrothermal copper and associated metals deposits in the Great Xing'an Range, NE China. Ore Geol. Rev. 61, 192–203.

Che, H.W., Zhou, Z.H., 2014. A preliminary study on the occurrence state and precipitation mechanism of gold in pyrite of Zhengguang Au Deposit. Acta Geol. Sinica (English Edition) 88 (Suppl. 2), 691–692.

Che, H.W., Zhou, Z.H., Ma, X.H., Ouyang, H.G., Liu, J., 2015. Geochemical characteristics, zircon U-Pb ages and Hf isotopic composition of the dacite porphyry from Zhengguang gold deposit in Northern great Xing'an Range. Acta Geol. Sinica 89 (8), 1417–1436 (in Chinese with English abstract).

Chen, B., Jahn, B.M., Wilde, S., Xu, B., 2000. Two contrasting Paleozoic magmatic belts in northern Inner Mongolia, China: petrogenesis and tectonic implications. Tectonophysics 328 (1), 157–182.

Chen, Z.G., Zhang, L.C., Lu, B.Z., Li, Z.L., Wu, H.Y., Xiang, P., Huang, S.W., 2010. Geochronology and geochemistry of the Taipingchuan copper-molybdenum deposit in Inner Mongolia and its geological significances. Acta Petrol. Sinica 26, 1437–1449 (in Chinese with English abstract).

Chen, Y.J., Zhang, C., Li, N., Yang, Y.F., Deng, K., 2012. Geology of the Mo deposits in Northeast China. J. Jilin Univ. (Earth Science Edition) 42 (5), 1223–1268 (in Chinese with English abstract).

Chu, S.X., Liu, J.M., Xu, J.H., Wei, H., Chai, H., Tong, K.Y., 2012. Zircon U-Pb dating, petrogenesis and tectonic significance of the granodiorite in the Sankuanggou skarn Fe-Cu deposit, Heilongjiang Province. Acta Petrol. Sinica 28 (2), 433–450 (in Chinese with English abstract).

Cui, W., 2006. Characters of orebodies in Zhengguang gold deposit, Heihe City, Heilongjiang Province. Sci. Technol. Inf. 22, 20 (in Chinese).

Cui, G., Wang, J.Y., Zhang, J.X., Cui, G., 2008. U-Pb SHRIMP dating of zircon from Duobaoshan granodiorite in Heilongjiang and its geological significance. Global Geol. 27 (4), 387–394 (in Chinese with English abstract).

Deng, K., Li, N., Yang, Y.F., Zhang, C., Yu, Y.B., Zhang, D.C., 2013. Fluid inclusion constraints on the origin of the Zhengguang gold deposit, Heihe City, Heilongjiang Province. Acta Petrol. Sinica 29 (1), 231–240 (in Chinese with English abstract).

Du, Q., Zhao, Y.M., Lu, B.G., Ma, D.Y., Li, P.L., Lv, J.K., Li, W.S., Ao, L.Z., Cui, G., 1988. Duobaoshan Porphyry Copper Deposit. Geological Publishing House, Beijing, pp. 1–369 (in Chinese).

Feng, J.X., 2008. Distribution character of sulfur isotope in the Duobaoshan copper deposit. Geol. Prospect. 44 (1), 46–49 (in Chinese with English abstract).

Feng, Z.Q., Jia, J., Liu, Y.J., Wen, Q.B., Li, W.M., Liu, B.Q., Xing, D.Q., Zhang, L., 2015. Geochronology and geochemistry of the Carboniferous magmatism in the northern Great Xing'an Range, NE China: constrains on the timing of amalgamation of Xing'an and Songnen blocks. J. Asian Earth Sci. 113, 411–426.

Fu, J.J., Zhao, Y.Y., Zeng, H., Li, Y., 2014. Chronological and isotopic characteristics of Zhengguang gold deposit in Heilongjiang Province, China. Acta Geol. Sinica (English Edition) 88 (supp.2), 718–719.

Fu, Y.L., Yang, Y.C., 2010. Deposit genesis prospecting criteria of Zhengguang gold deposit, Heilongjiang. Gold 31 (6), 13–18 (in Chinese with English abstract).

Gao, R.Z., Lv, X.B., Yang, Y.S., Li, C.C., 2014a. Characteristics of cryptoexplosive Breccia in Zhengguang gold deposit of Heilongjiang Province and its geological implication. Geol. Explor. 50 (5), 874–883 (in Chinese with English abstract).

Gao, R.Z., Lv, X.B., Yang, Y.S., Li, C.C., 2014b. Fluid inclusion study of Zhengguang gold deposit in Heilongjiang province and its ore genesis discussion. Acta Geol. Sinica (English Edition) 88 (supp.2), 720–721.

Ge, W.C., Wu, F.Y., Zhou, C.Y., Zhang, J.H., 2007. Porphyry Cu-Mo deposits in the eastern Xing'an-Mongolian Orogenic Belt: mineralization ages and their geodynamic implications. Chin. Sci. Bull. 52 (4), 3416–3427 (in Chinese).

Goldfarb, R.J., Taylor, R.D., Collins, G.S., Goryachev, N.A., Orlandini, O.F., 2014. Phanerozoic continental growth and gold metallogeny of Asia. Gondwana Res. 25 (1), 48–102.

Gou, J., Sun, D.Y., Ren, Y.S., Liu, Y.J., Zhang, S.Y., Fu, C.L., Wang, T.H., Wu, P.F., Liu, X. M., 2013. Petrogenesis and geodynamic setting of Neoproterozoic and Late Paleozoic magmatism in the Manzhouli-Erguna area of Inner Mongolia, China: geochronological, geochemical and Hf isotopic evidence. J. Asian Earth Sci. 67–68, 114–137.

Han, Z.X., Xu, Y.Q., Zheng, Q.D., 2004. Metallogenetic Series and Evolution of Significant Metal and Nonmetal Mineral Resources in Heilongjiang Province. Heilongjiang People's Publishing House, Harbin, pp. 1–241 (in Chinese with English abstract).

Han, C.M., Wang, C.B., Li, Z.M., Chang, X.X., Ma, D.Y., Li, C.Y., 2007. The Resource Potential in the Duobaoshan Ore Deposit. Geological Publishing House, Beijing, pp. 1–127 (in Chinese).

Hao, Y.J., Ren, Y.S., Duan, M.X., Tong, K.Y., Chen, C., Yang, Q., Li, C., 2015. Metallogenic events and tectonic setting of the Duobaoshan ore field in Heilongjiang Province, NE China. J. Asian Earth Sci. 97, 442–458.

Hoefs, J., 1997. Stable Isotope Geochemistry. Springer-Verlag, Berlin, pp. 1-250.

Hu, X.L., Ding, Z.J., He, M.C., Yao, S.Z., Zhu, B.P., Shen, J., Chen, B., 2014a. Two epochs of magmatism and metallogeny in the Cuihongshan Fe-polymetallic deposit, Heilongjiang Province, NE China: constrains from U-Pb and Re-Os geochronology and Lu-Hf isotopes. J. Geochem. Explor. 143, 116–126.

Hu, X.L., Ding, Z.J., He, M.C., Yao, S.Z., Zhu, B.P., Shen, J., Chen, B., 2014b. A porphyry-skarn metallogenic system in the lesser Xing'an range, NE China: implications from U-Pb and Re-Os geochronology and Sr-Nd-Hf isotopes of the Luming Mo and Xulaojiugou Pb-Zn deposits. J. Asian Earth Sci. 90, 88–100.

Hu, X.L., Yao, S.Z., He, M.C., Ding, Z.J., Cui, Y.B., Shen, J., Chen, B., Zhu, B.P., 2014c. Geochemistry, U-Pb geochronology and Hf isotope studies of the Daheishan porphyry Mo deposit in Heilongjiang Province, NE China. Resour. Geol. 64, 102–116.

Hu, X.L., Yao, S.Z., Ding, Z.J., He, M.C., 2016. Early Paleozoic magmatism and metallogeny in Northeast China: a record from the Tongshan porphyry Cu deposit. Miner. Deposita, 1–19.

Jia, D.C., Hu, R.Z., Lu, Y., Qiu, X.L., 2004. Collision belt between the Khanka block and the North China block in the Yanbian Region, Northeast China. J. Asian Earth Sci. 23, 211–219.

Li, J.Y., 1998. Some new ideas on tectonics of NE China and its neighboring areas. Geol. Rev. 44 (4), 339–347 (in Chinese with English abstract).

Li, D.R., 2011. Metallogenic Laws and Prospecting Direction in the Sankuanggou Copper Poly-metallic Mining Area (Deposit), Heilongjiang Province (PhD Thesis). China University of Geosciences (Beijing), Beijing, pp. 1–146 (in Chinese with English abstract).

Li, Y., Fu, J.J., Zhao, Y.Y., Zeng, H., 2016. Chronological characteristics and metallogenic significance of Zhengguang gold deposit, Heilongjiang Province, China. Acta Geol. Sinica 90 (1), 151–162 (in Chinese with English abstract).

Liang, H.Y., Sun, W.D., Su, W.C., Zartman, R.E., 2009. Porphyry copper-gold mineralization at Yulong, China, promoted by decreasing redox potential during magnetite alteration. Econ. Geol. 104 (4), 587–596.

Liu, Y.S., Hu, Z.C., Gao, S., Gunther, D., Xu, J., Gao, C.G., Chen, H.H., 2008. In situ analysis of major and trace elements of anhydrous minerals by LA-ICPMS without applying an internal standard. Chem. Geol. 257, 34–43.

Liu, J., Wu, G., Zhong, W., Zhu, M.T., 2010a. Fluid inclusion study of the Duobaoshan porphyry Cu (Mo) deposit Heilongjiang province, China. Acta Petrol. Sinica 26 (5), 1450–1464 (in Chinese with English abstract).

Liu, Y.J., Zhang, X.Z., Jin, W., Chi, X.G., Wang, C.W., Ma, Z.H., Han, G.Q., Wen, Q.B., Li, W., Wang, W.D., Zhao, X.F., 2010b. Late Paleozoic tectonic evolution in northeast China. Geol. China 37 (4), 943–951 (in Chinese with English abstract).

Liu, Y.S., Gao, S., Hu, Z., Gao, C., Zong, K., Wang, D., 2010c. Continental and oceanic crust recycling-induced melt-peridotite interactions in the Trans-North China Orogen: U-Pb dating, Hf isotopes and trace elements in zircons of mantle xenoliths. J. Petrol. 51, 537–571.

Liu, J., Wu, G., Li, Y., Zhu, M.T., Zhong, W., 2012. Re-Os sulfide (chalcopyrite, pyrite and molybdenite) systematic and fluid inclusion study of the Duobaoshan porphyry Cu (Mo) deposit, Heilongjiang Province, China. J. Asian Earth Sci. 49, 300–312.

Liu, J., Zhou, Z.H., He, Z.F., Ouyang, H.G., 2015. Zircon U-Pb dating and geochemistry of ore-bearing tonalite in Tongshan copper deposit, Heilongjiang Province. Miner. Deposits 34 (2), 289–308 (in Chinese with English abstract).

Lu, J.H., Liu, X.P., 2009. Ore genesis and prospecting criteria of Zhengguang gold deposit, Heilongjiang. Technol. Inf. Heilongjiang 9, 14 (in Chinese).

Lu, H., Sun, X.X., 2015. Application of Micromine to exploration of II ore zone in Zhengguang gold deposit, Heilongjiang Province. Contrib. Geol. Miner. Resour. Res. 30 (2), 261–266 (in Chinese with English abstract).

Ludwig, K.R., 2003. ISOPLOT 3.00: A Geochronological Toolkit for Microsoft Excel. Berkeley Geochronology Center, Berkeley, California, pp. 39.

Ma, D.Y., 1984. Isotope Geology of the Duobaoshan Copper Ore Field. Miner. Deposits 3 (1), 47–57 (in Chinese with English abstract).

Mao, J.W., Pirajno, F., Lehmann, B., Luo, M., Berzina, A., 2014. Distribution of porphyry deposits in the Eurasian continent and their corresponding tectonic settings. J. Asian Earth Sci. 79, 576–584.

Mao, J.W., Xie, G.Q., Bierlein, F., Qu, W.J., Du, A.D., Ye, H.S., Pirajno, F., Li, H.M., Guo, B. J., Lie, Y.F., Yang, Z.Q., 2008. Tectonic implications from Re-Os dating of Mesozoic molybdenum deposits in the east Qinling-Dabie orogenic belt. Geochim. Cosmochim. Acta 72, 4607–4626.

Mei, W., Lü, X., Cao, X., Liu, Z., Zhao, Y., Ai, Z., Tan, R., Abfaua, M.M., 2015. Ore genesis and hydrothermal evolution of the Huanggang skarn iron–tin poly-metallic deposit, southern Great Xing'an Range: evidence from fluid inclusions and isotope analyses. Ore Geol. Rev. 64, 239–252.

Ouyang, H.G., Mao, J.W., Santosh, M., Zhou, J., Zhou, Z.H., Wu, Y., Hou, L., 2013. Geodynamic setting of Mesozoic magmatism in NE China and surrounding regions: perspectives from spatio-temporal distribution patterns of ore deposits. J. Asian Earth Sci. 78, 222–236.

Pirajno, F., 2010. Intracontinental strike-slip faults, associated magmatism, mineral systems and mantle dynamics: examples from NW China and Altay-Sayan (Siberia). J. Geodyn. 50 (3), 325–346.

Qu, H., Li, C.L., Zhao, Z.H., Wang, Z., Zhang, J.F., 2011. Zircon U-Pb ages and geochemical characteristics of the granites in Duobaoshan area, Northeast Da Hinggan Mountains. Geol. China 38 (2), 292–300 (in Chinese with English abstract).

Ren, J.S., Chen, T.Y., Niu, B.G., Liu, Z.G., Liu, E.R., 1990. Tectonic Evolution of the Continental Lithosphere and Metallogeny in Eastern China and Adjacent Areas. Science Press, Beijing, pp. 1–205 (in Chinese).
Ren, J.S., Wang, Z.X., Chen, B.W., Jiang, C.F., Niu, B.G., Li, J.Y., Xie, G.L., He, Z.J., Liu, Z. G., 1997. A new generation tectonic map of China. Regional Geol. China 16 (3), 225–230 (in Chinese with English abstract).
Reynolds, P., Ravenhurst, C., Zentilli, M., Lindsay, D., 1998. High-precision $^{40}Ar/^{39}Ar$ dating of two consecutive hydrothermal events in the Chuquicamata porphyry copper system, Chile. Chem. Geol. 148, 45–60.
Richards, J.P., 2011. Magmatic to hydrothermal metal fluxes in convergent and collided margins. Ore Geol. Rev. 40, 1–26.
Robinson, P.T., Zhou, M.F., Hu, X.F., Reynolds, P., Wenji, B., Yang, J., 1999. Geochemical constraints on the origin of the Hegenshan Ophiolite, Inner Mongolia, China. J. Asian Earth Sci. 17 (4), 423–442.
Rye, R.O., 1993. The evolution of magmatic fluids in the epithermal environment: the stable isotope perspective. Econ. Geol. 88 (3), 733–753.
Seltmann, R., Porter, T.M., Pirajno, F., 2014. Geodynamics and metallogeny of the central Eurasian porphyry and related epithermal mineral systems: a review. J. Asian Earth Sci. 79, 810–841.
Sengör, A.M.C., Natal'In, B.A., Burtman, V.S., 1993. Evolution of the Altaid tectonic collage and Palaeozoic crustal growth in Eurasia. Nature 364, 299–307.
Selby, D., Creaser, R.A., 2001. Re-Os geochronology and systematics in molybdenite from the Endako porphyry molybdenum deposit, British Columbia, Canada. Econ. Geol. 96, 197–204.
She, H.Q., Li, J.W., Xiang, A.P., Guan, J.D., Yang, Y.C., Zhang, D.Q., Tan, G., Zhang, B., 2012. U-Pb ages of the zircons from primary rocks in middle-northern Daxinganling and its implications to geotectonic evolution. Acta Petrol. Sinica 28 (2), 571–594 (in Chinese with English abstract).
Shen, J., He, M., Ding, Z., 2014. Geological characteristics and discussion on metallogenic epoch of Zhengguang Gold Deposit, Heihe City, Heilongjiang Province. Acta Geol. Sinica (English Edition) 88 (Suppl. 2), 599–600.
Sillitoe, R.H., 2010. Porphyry copper systems. Econ. Geol. 105, 3–41.
Song, G.X., Qin, K.Z., Wang, L., Guo, J.H., Li, Z.Z., Dong, K.Y., Zou, X.Y., Li, G.M., 2015. Type, zircon U-Pb age and Paleo-volcani edifice of Zhengguang gold deposit in Duobaoshan ore field in Heilongjiang Province, NE-China. Acta Petrol. Sinica 31 (8), 2402–2416 (in Chinese with English abstract).
Sun, W.D., Arculus, R.J., Kamenetsky, V.S., Binns, R.A., 2004. Release of gold-bearing fluids in convergent margin magmas prompted by magnetite crystallization. Nature 431 (7011), 975–978.
Sun, W.D., Liang, H.Y., Ling, M.X., Zhan, M.Z., Ding, X., Zhang, H., Yang, X.Y., Li, Y.L., Ireland, T.R., Wei, Q.R., Fan, W.M., 2013. The link between reduced porphyry copper deposits and oxidized magmas. Geochim. Cosmochim. Acta 103, 263–275.
Sun, W.D., Huang, R.F., Li, H., Hu, Y.B., Zhang, C.C., Sun, S.J., Zhang, L.P., Ding, X., Li, C. Y., Zartman, R.E., Ling, M.X., 2015. Porphyry deposits and oxidized magmas. Ore Geol. Rev. 65, 97–131.
Tong, K.Y., Yang, Y.C., Song, G.X., Liang, H.J., Ma, L.F., 2015. Geological characteristics, genesis and prospecting potential of the Zhengguang Au-Zn Deposit in Heilongjiang Province. Geol. Explor. 51 (3), 507–518 (in Chinese with English abstract).
Wang, H.Z., Mo, X.X., 1995. An outline of the tectonic evolution of China. Episodes 18, 6–16.
Wang, X.C., Wang, X.L., Wang, L., Liu, J.Y., Xia, B., Deng, J., Xu, X.M., 2007. Metallogeny and reformation of the Duobaoshan super large porphyry copper deposit in Heilongkiang province. Chin. J. Geol. 42 (1), 124–133 (in Chinese with English abstract).
Wang, Y.H., Xue, C.J., Liu, J.J., Wang, J.P., Yang, J.T., Zhang, F.F., Zhao, Z.N., Zhao, Y.J., 2014. Geochemistry, geochronology, Hf isotope, and geological significance of the Tuwu porphyry copper deposit in eastern Tianshan, Xinjiang. Acta Petrol. Sinica 30 (11), 3383–3399 (in Chinese with English abstract).
Wang, Y.H., Zhao, C.B., Zhang, F.F., Liu, J.J., Wang, J.P., Peng, R.M., Liu, B., 2015. SIMS zircon U-Pb and molybdenite Re–Os geochronology, Hf isotope, and whole-rock geochemistry of the Wunugetushan porphyry Cu–Mo deposit and granitoids in NE China and their geological significance. Gondwana Res. 28 (3), 1228–1245.
Wu, F.Y., Sun, D.Y., Li, H.M., Wang, X.L., 2001. The nature of basement beneath the Songliao Basin in NE China: geochemical and isotopic constrains. Phys. Chem. Earth Part A. 26, 793–803.
Wu, F.Y., Sun, D.Y., Li, H.M., Jahn, B.M., Wilde, S., 2002. A-type granites in northern China: age and geochemical constraints on their petrogenesis. Chem. Geol. 187 (1), 143–173.
Wu, G., Sun, F.Y., Zhao, C.S., Li, Z.T., Zhao, A.L., Pang, Q.B., Li, G.Y., 2005. Discovery of the Early Paleozoic post-collosional granites in northern margin of the Ergun massif and its geological significance. Chin. Sci. Bull. 50 (23), 2733–2743 (in Chinese).
Wu, Z.Y., Sun, Y.C., Wang, B.Q., 2006. Geology and geochemistry of Zhengguang gold deposit, Heilongjiang Province. Geol. Prospect. 42 (1), 38–42 (in Chinese with English abstract).
Wu, G., Liu, J., Zhong, W., Zhu, M.T., Mei, M., Wan, Q., 2009. Fluid inclusion study of the Tongshan porphyry copper deposit, Heilongjiang Province, China. Acta Petrol. Sinica 25 (11), 2995–3006 (in Chinese with English abstract).
Wu, F.Y., Sun, D.Y., Ge, W.C., Zhang, Y.B., Grant, M.L., Wilde, S.A., Jahn, B.M., 2011. Geochronology of the Phanerozoic granitoids in northeastern China. J. Asian Earth Sci. 41 (1), 1–30.
Wu, C., Jiang, T., Liu, C., Liu, W., 2014. Early Cretaceous A-type granites and Mo mineralization, Aershan area, eastern Inner Mongolia, Northeast China: geochemical and isotopic constraints. Int. Geol. Rev. 56 (11), 1357–1376.
Xiang, A.P., Yang, Y.C., Li, G.T., She, H.Q., Guan, J.D., Li, J.W., Guo, Z.J., 2012. Diagenetic and metallogenic ages of Duobaoshan porphyry Cu-Mo deposit in Heilongjiang Province. Miner. Deposits 31 (6), 1237–1248 (in Chinese with English abstract).
Xiao, W., Windley, B.F., Allen, M.B., Han, C., 2013. Paleozoic multiple accretionary and collisional tectonics of the Chinese Tianshan orogenic collage. Gondwana Res. 23 (4), 1316–1341.
Xiao, W., Windley, B.F., Hao, J., Zhai, M., 2003. Accretion leading to collision and the Permian Solonker suture, Inner Mongolia, China: termination of the central Asian orogenic belt. Tectonics 22 (6), 1–20.
Xu, W.L., Ji, W.Q., Pei, F.P., Meng, E., Yu, Y., Yang, D.B., Zhang, X., 2009. Triassic volcanism in eastern Heilongjiang and Jilin Provinces, NE China: chronology, geochemistry, and tectonic implications. J. Asian Earth Sci. 34 (3), 392–402.
Zartman, R.E., Doe, B.R., 1981. Plumbotectonics-the model. Tectonophysics 75 (1), 135–162.
Zeng, Q.D., Liu, J.M., Chu, S.X., Wang, Y.B., Sun, Y., Duan, X.X., Zhou, L.L., Qu, W.L., 2014. Re-Os and U-Pb geochronology of the Duoshan porphyry Cu-Mo-(Au) deposit, Northeastern China, and its geological significance. J. Asian Earth Sci. 79, 895–909.
Zhang, B.L., 2004. The newly discovered high grade epithermal gold deposit in Northern Heilongjiang Province: Zhengguang gold mine. Gold Sci. Technol. 12 (6), 46 (in Chinese).
Zhang, Y.F., Li, G.D., Yan, B.C., Wang, J.M., 2011. Geological features and genesis of Zhengguang gold deposit, Heilongjiang Province. Jilin Geol. 30 (1), 41–43 (in Chinese with English abstract).
Zhang, F.F., Wang, Y.H., Liu, J.J., Wang, J.P., Zhao, C.B., Song, Z.W., 2016. Origin of the Wunugetushan porphyry Cu-Mo deposit, Inner Mongolia, NE China: constraints from geology, geochronology, geochemistry, and isotopic compositions. J. Asian Earth Sci. 117, 208–224.
Zhao, Y.M., Zhang, D.Q., 1997a. Metallogeny and Prospective Evolution of Copper-poly-metallic Deposit in the Da Hinggan Mountains and its Adjacent Regions. Seismological Press, Beijing, pp. 318 (in Chinese).
Zhao, Y.M., Bi, C.S., Zou, X.Q., Sun, Y.L., Du, A.D., 1997b. The Re-Os isotope age of molybdenite from Duobaoshan and Tongshan porphyry copper (molybdenum) deposits. Acta Geosci. Sinica 18 (1), 61–67 (in Chinese with English abstract).
Zhao, G.J., Hou, Y.S., Wang, B.Q., 2006. Geological characteristics and genesis of Zhengguang gold deposit in Heilongjiang Province. Non-Ferrous Min. Metall. 22 (3), 3–6 (in Chinese with English abstract).
Zhao, G.J., Huo, Y.S., Ceng, F.Q., 2007. Geological characteristics and genisis of Zhengguang gold deposit in Heihe city of Heilongjiang province. Nonferrous Metals 59 (3), 91–94 (in Chinese with English abstract).
Zhao, Y.Y., Wang, J.P., Zhao, G.J., Cui, Y.B., 2011a. Metallogenic regularity and prospecting direction of Duobaoshan ore field, Heilongjiang Province, China. J. Jilin Univ. (Earth Science Edition) 41 (6), 1676–1688 (in Chinese with English abstract).
Zhao, H.L., Liu, X.G., Liu, H.Y., Zhu, C.Y., 2011b. Petrological evidence of Paleozoic marine basin closure in Duobaoshan of Heilongjiang. Global Geol. 30 (1), 18–27 (in Chinese with English abstract).
Zhao, T.Y., Zhao, H.B., Sun, F.Y., Liu, J.L., 2013. Metallogenic epoch of the Sandaowanzi gold deposit in Heilongjiang Province: constraints from the evidence of isotopic age. Geol. China 40 (4), 1202–1208 (in Chinese with English abstract).
Zhao, X., Xue, C., Chi, G., Pak, N., Zu, B., 2015. Re-Os pyrite and U-Pb zircon geochronology from the Taldybulak Levoberezhny gold deposit: Insight for Cambrian metallogeny of the Kyrgyz northern Tien Shan. Ore Geol. Rev. 67, 78–89.
Zheng, Q.B., 2012. Geological Characteristics and Ore Genesis of Zhengguang Gold Deposit in Heihe area, Heilongjiang Province (Master Degree Thesis). Jilin University, Changchun, pp. 1–45 (in Chinese with English abstract).
Zhou, J.B., Wilde, Simon A., Zhang, X.Z., Ren, S.M., Zheng, C.Q., 2011. Early Paleozoic metamorphic rocks of the Erguna block in the Great Xing'an Range, NE China: evidence for the timing of magmatic and metamorphic events and their tectonic implications. Tectonophysics 499 (1), 105–117.